12-2022

A Framework for Assessing The 4th Rank Dispersivity Tensor Under Anisotropic Axial Symmetries

Xiang Fan
Western Michigan University

A FRAMEWORK FOR ASSESSING THE 4TH RANK DISPERSIVITY TENSOR UNDER ANISOTROPIC AXIAL SYMMETRIES

Xiang Fan, Ph.D.

Western Michigan University, 2022

Multi-dimensional expansion of the advection-dispersion equation necessitated the representation of dispersivity as a 4^{th} rank tensor. This tensorial form of dispersivity has 81 terms in three-dimensions with a maximum of 36 independent terms that may be used to describe Fickian spreading of a dissolved contaminant plume according to intrinsic properties of a porous medium. The complexity of the 4^{th} rank tensor has led to the common practice of simplifying the tensor to only 2 or 3 independent terms by assuming isotropic conditions, although isotropic porous media are uncommon in nature as many natural geologic systems exhibit pronounced anisotropy. A broad set of crystallographic symmetries are investigated for application to the dispersivity tensor. Listed in order of high to low symmetry, these symmetries include isotropic, hexagonal, tetragonal, orthorhombic, monoclinic, and triclinic. A framework is developed for each of these symmetries to identify and quantify connections between individual dispersivity terms with principal values of the 2^{nd} rank dispersion tensor. A sensitivity analysis is performed to determine the influence of individual terms of dispersivity on principal components of dispersion. A numerical method allowing for visualization of resultant multi-Gaussian densities for any of these axial symmetries is also presented. Conservative particle transport in lattice networks is used to parameterize the full dispersivity tensor for hexagonal, tetragonal, and orthorhombic symmetries.

A FRAMEWORK FOR ASSESSING THE 4TH RANK DISPERSIVITY TENSOR UNDER ANISOTROPIC AXIAL SYMMETRIES

by

Xiang Fan

A dissertation submitted to the Graduate College
in partial fulfillment of the requirements
for the degree of Doctor of Philosophy
Statistics
Geological and Environmental Sciences
December 2022

Doctoral Committee:

Donald M. Reeves, Ph.D., Chair
Daniel Patrick Cassidy, Ph.D.
Duane Hampton, Ph.D.
Melinda Koelling, Ph.D.

ACKNOWLEDGMENTS

I would like to express my gratitude to Dr. Donald M. Reeves, the chair of my doctoral committee. Thank you for your continuously patience, help and advising for the past five years. I would also want to thank you for my doctoral committee members: Dr Dan Cassidy, Dr Duane Hampton, and Dr. Melinda Koelling for their support and advice. Especially for Dr. Melinda Koelling, she agreed to serve as my committee member when I had to find a new committee member just one month before the defense. That really helped me a lot. Finally, I want to thank you for my parent for their support and love.

Xiang Fan

TABLE OF CONTENTS

ACKNOWLEDGMENTS ii

LIST OF TABLES vi

LIST OF FIGURES vii

CHAPTER

1. INTRODUCTION 1

2. BUILDING RELATIONSHIPS AMONG DISPERSION, DISPERSIVITY AND VELOCITY 7

    2.1 Prerequisites 9

    2.2 Expressions and Validations 12

    2.3 Calculation 13

        2.3.1 Two-Dimensional General Case (Triclinic) 13

        2.3.2 Hexagonal 14

        2.3.3 Tetragonal 14

        2.3.4 Orthorhombic 15

3. SENSITIVITY ANALYSIS 16

    3.1 Hexagonal, Tetragonal, and Orthorhombic Symmetry 16

    3.2 Generalization to All Symmetries 20

Table of Contents—Continued

4. MULTIVARIATE GAUSSIAN VISUALIZATION AND TENSOR APPLICATION....24
4.1 Plume Visualization for Axial Symmetries....25
4.1.1 Isotropic....26
4.1.2 Hexagonal....26
4.1.3 Tetragonal....27
4.1.4 Orthorhombic....27
4.1.5 Monoclinic....27
4.1.6 Triclinic....28
4.2 Application of Anisotropic Tensor to Numerical Data....29
4.2.1 Hexagonal/Tetragonal....32
4.2.2 Orthorhombic....33
5. DISCUSSION....37
6. CONCLUSION AND FUTURE WORK....39
6.1 Conclusion....39
6.2 Future Work....40
6.2.1 Numerical Simulation on Hexagonal, Monoclinic and Triclinic Symmetries....40
6.2.2 Borden Landfill....40

Table of Contents—Continued

APPENDICES

A.DISPERSION VALUES 42

B.VALIDATION PROCESS 47

REFERENCES 51

LIST OF TABLES

1. Impact of each single dispersivity variable to dispersion value for (1a) hexagonal symmetry, (1b) tetragonal symmetry, and (1c) orthorhombic symmetry. 19

2. Parameter sets used to generate lattice networks for hexagonal-tetragonal and orthorhombic systems 32

LIST OF FIGURES

1. Example of crystal system. 9

2: Sensitivity analysis of the principal components of the dispersion tensor to dispersivity tensor values. 18

3: Three-dimensional plume (multi-Gaussian density) after some elapsed time resulting from an instantaneous point injection of a conservative solute.. 25

4: Shape of the plume. 29

5: Numerical simulation of particle transport through hexagonal-tetragonal system.....35

6: Numerical simulation of particle transport through orthorhombic system. 36

CHAPTER I

INTRODUCTION

Solute transport in groundwater flow systems is governed by the processes of advection and dispersion, which describe a dissolved solute moving at the rate of the average groundwater velocity, and solute spreading in a porous medium due to the combined effects of velocity variations and pathway tortuosity, respectively. These processes are mathematically defined in the advection-dispersion equation (ADE) (Scheidegger, 1957; Bear, 1961):

$$\frac{\partial C}{\partial t} = -\nabla \cdot (vC) + \nabla \cdot (D\nabla C) \quad (1)$$

where C is solute concentration [M/L^3], D is the Fickian dispersion coefficient [L^2/T], v is groundwater velocity [L/T], and t is time [T]. Velocity and dispersion coefficients are both 2nd rank tensors.

Derivations of the multi-dimensional form of the ADE posed some challenges in how to mathematically model dispersion. For example, in one-dimensional forms of the ADE, a relationship was proposed to connect velocity to the dispersion coefficient (Scheidegger, 1954, 1958; Day, 1956; Rifai et al, 1956):

$$D = a \cdot v \quad (2)$$

where a [L] is dispersivity and describes the intrinsic spreading properties of the porous media. All parameters in Eq. 2 are scalar in one-dimension, yet are tensors in multi-dimensional form. Specifically, since velocity and dispersion are 2nd rank tensors in Eq. 1, dispersivity, which is defined in Eq. 2 as a linear function of velocity and dispersion, must also be a tensor of 4th rank (Bear, 1961; Scheidegger, 1961).

Bear (1961) defined the multi-dimensional form of Eq. 2:

$$D_{ij} = a_{ijkl} \frac{v_k v_l}{v} \quad (3)$$

where a_{ijkl} is the 4th rank dispersivity tensor, and $v_k v_l$ is the inner (dyadic) product of velocity vector v (a 2nd rank tensor), and D_{ij} is the 2nd rank dispersion tensor:

$$D_{ij} = \begin{vmatrix} D_{11} & D_{12} & D_{13} \\ D_{12} & D_{22} & D_{23} \\ D_{13} & D_{23} & D_{33} \end{vmatrix}. \quad (4)$$

D_{ij} should be positive definite matrix (Fel and Bear, 2009). It has following constraint conditions:

$$\begin{matrix} det\,|D_{11}| > 0 \\ det \begin{vmatrix} D_{11} & D_{12} \\ D_{12} & D_{22} \end{vmatrix} > 0 \\ det \begin{vmatrix} D_{11} & D_{12} & D_{13} \\ D_{12} & D_{22} & D_{23} \\ D_{13} & D_{23} & D_{33} \end{vmatrix} > 0 \end{matrix}.$$

This constraint conditions can also be expressed as: $\begin{cases} \lambda_1 > 0 \\ \lambda_2 > 0 \\ \lambda_3 > 0 \end{cases}$, where λ_1, λ_2, λ_3 are the eigenvalues of matrix 4.

Combining Eq. 1 and 3 results in (Bear, 1961, 1972):

$$\frac{\partial C}{\partial t} = -v_i \frac{\partial C}{\partial x_i} + \frac{\partial}{\partial x_i} a_{ijkl} \frac{v_l v_m}{v} \frac{\partial C}{\partial x_j}. \quad (5)$$

A 4th rank tensor on a Cartesian coordinate system contains $3^4 = 81$ terms. However, the 4th rank dispersivity tensor a_{ijkl} belongs to the symmetry group $[V^2]^2$ because of its inherent symmetries and has two pairs of indices: (Scheidegger, 1961):

$$a_{ijkl} = a_{jikl} = a_{ijlk}. \quad (6)$$

Hence, dispersivity can be simplified to a 6 x 6 matrix with 36 components:

$$a_{pq} \cong a_{ijkl} = \begin{vmatrix} a_{11} & a_{12} & a_{13} & a_{14} & a_{15} & a_{16} \\ a_{21} & a_{22} & a_{23} & a_{24} & a_{25} & a_{26} \\ a_{31} & a_{32} & a_{33} & a_{34} & a_{35} & a_{36} \\ a_{41} & a_{42} & a_{43} & a_{44} & a_{45} & a_{46} \\ a_{51} & a_{52} & a_{53} & a_{54} & a_{55} & a_{56} \\ a_{61} & a_{62} & a_{63} & a_{64} & a_{65} & a_{66} \end{vmatrix} \quad (7)$$

where $a_{pq} \cong a_{ijkl}$, $ij \ll p = 1,2,3,4$, $kl \ll q = 1,2,3,4$. Values of a_{ijkl} should satisfy the constraint conditions in matrix 4. Matrix 7 represents the most general case of the dispersivity tensor.

The use of 4th rank tensor is relatively uncommon in science and engineering. One similar example to the dispersivity tensor is Hooke's law:

$$\sigma_{ij} = c_{ijkl}\varepsilon_{kl} \quad (8)$$

where σ_{ij} is the 2nd rank stress tensor, c_{ijkl} is the 4th rank elasticity tensor, and e_{kl} is the 2nd rank strain tensor. Dispersivity and elasticity also share a similar one-dimension linear relationship: $F = -k \cdot x$, where k is spring constant, F is force, and x is change in length. However, one major difference between the elasticity c_{ijkl} and dispersivity tensors a_{ijkl} is that the elasticity tensor has higher inherent symmetries and follows the symmetry group $[[V^2]^2]$. This leads to two pairs of indices under permutation (Sirotin and Shaskolskaia, 1982):

$$c_{ijkl} = c_{jikl} = c_{ijlk} = c_{klij}. \quad (9)$$

Thus, the elasticity tensor may contain a maximum 21 independent terms in three-dimensions, while the dispersivity tensor may contain up to 36 independent terms.

Components of the dispersivity tensor can be defined for various axial symmetries adopted from crystallography (Sirotin and Shaskolskaia, 1982). Presented in the order of higher to lower axial symmetry, these axial symmetries include isotropic, hexagonal, tetragonal, orthorhombic, monoclinic, and triclinic cases. In general, the complexity of the tensor is represented by the number of non-zero terms. The dispersivity tensor was first investigated by assuming isotropic symmetry (Bear, 1961):

$$a_{pq} \cong a_{ijkl} = \begin{vmatrix} a_{11} & a_{12} & a_{12} & 0 & 0 & 0 \\ a_{12} & a_{11} & a_{12} & 0 & 0 & 0 \\ a_{12} & a_{12} & a_{11} & 0 & 0 & 0 \\ 0 & 0 & 0 & \frac{1}{2}(a_{11} - a_{12}) & 0 & 0 \\ 0 & 0 & 0 & 0 & \frac{1}{2}(a_{11} - a_{12}) & 0 \\ 0 & 0 & 0 & 0 & 0 & \frac{1}{2}(a_{11} - a_{12}) \end{vmatrix}. \quad (10)$$

where a_{11} is defined as longitudinal dispersivity and a_{12} is transverse dispersivity which describe the spreading of a three-dimensional Gaussian plume both along and transverse to the average direction of groundwater flow, respectively. With only 2 independent components, matrix 10 is can be expressed in Einstein notation:

$$a_{pq} \cong a_{ijkl} = a_T \delta_{ij} \delta_{kl} + \frac{(a_L - a_T)}{2} \left(\delta_{ik} \delta_{jl} + \delta_{il} \delta_{jk} \right) \quad (11)$$

where δ_{ij} is the Kronecker delta function: $\delta_{ij} = \begin{cases} 1, if\ i = j \\ 0, if\ i \neq j \end{cases}$.

While isotropic symmetry is an ideal condition, it rarely occurs in geologic systems which often exhibit pronounced asymmetry. Examples include unconsolidated aquifers comprised of sediment deposited in horizontal or near-horizontal layers with different characteristic grain sizes and permeabilities that lead to vertical anisotropy (Pickup et al, 1994); disordered systems such as rock fracture networks and alluvial aquifers where permeability has a directional dependence (Oda et al, 1987; Lee et al, 2007; Klimczak et al, 2010); and fault damage zones in crystalline or metamorphic rock which focus fluid flow and solute transport parallel to the fault (Bruhn et al, 1994; Caine et al, 1996; Johri et al, 2014).

Most recently, Fel and Bear (2009) recognized limitations of the symmetric dispersivity tensor and developed a cursory framework that incorporates hexagonal and tetragonal axial symmetries in the dispersivity tensor. For hexagonal symmetry in three-dimensions, the dispersivity tensor has 6 non-zero elements (Sirotin and Shaskolskaia, 1982):

$$a_{pq} \cong a_{ijkl} = \begin{vmatrix} a_{11} & a_{12} & a_{13} & 0 & 0 & 0 \\ a_{12} & a_{11} & a_{13} & 0 & 0 & 0 \\ a_{31} & a_{31} & a_{33} & 0 & 0 & 0 \\ 0 & 0 & 0 & a_{44} & 0 & 0 \\ 0 & 0 & 0 & 0 & a_{44} & 0 \\ 0 & 0 & 0 & 0 & 0 & \frac{1}{2}(a_{11} - a_{12}) \end{vmatrix}. \quad (12)$$

The dispersivity tensor in the case of tetragonal symmetry is slightly more complex than the hexagonal case, and contains 7 non-zero elements (Sirotin and Shaskolskaia, 1982):

$$a_{pq} \cong a_{ijkl} = \begin{vmatrix} a_{11} & a_{12} & a_{13} & 0 & 0 & 0 \\ a_{12} & a_{11} & a_{13} & 0 & 0 & 0 \\ a_{31} & a_{31} & a_{33} & 0 & 0 & 0 \\ 0 & 0 & 0 & a_{44} & 0 & 0 \\ 0 & 0 & 0 & 0 & a_{44} & 0 \\ 0 & 0 & 0 & 0 & 0 & a_{55} \end{vmatrix}. \quad (13)$$

Bear et al (2009) utilized eigenvectors to denote directions of the symmetry axes and eigenvalues to describe the rates of spreading along the eigenvectors. Using this methodology, the hexagonal case of the dispersivity tensor can be expressed as (Fel and Bear, 2009):

$$a_{pq} \cong a_{ijkl} = a_1\delta_{ij}\delta_{kl} + \frac{a_2}{2}\left(\delta_{ik}\delta_{jl} + \delta_{il}\delta_{jk}\right) + a_3 e_i e_j \delta_{kl} + a_4 e_k e_l \delta_{ij} + \frac{a_5}{2}\left(e_i e_k \delta_{jl} + e_j e_k \delta_{il} + e_i e_l \delta_{jk} + e_j e_l \delta_{ik}\right) + a_6 e_i e_j e_k e_l \quad (14)$$

where a_1 to a_6 represent tensor values for a_{11} to a_{44} in matrix 12, e_i, e_j, e_k, e_l are eigenvalues, and δ_{ij} is the Kronecker delta function. Similarly, the tetragonal symmetry case can be represented in eigenvector and eigenvalue form as (Fel and Bear, 2009):

$$D_{ij}.v = \left(a_1((\alpha_k V_k)^2 + (\beta_k V_k)^2)\right) + a_2 v^2)\delta_{ij} + (a_3((\alpha_k V_k)^2 + (\beta_k V_k)^2)) + a_4 v^2)\left(\alpha_i\alpha_j + \beta_i\beta_j\right) + a_5\left((\alpha_k V_k)\left(\alpha_i V_j + \alpha_j V_i\right) + (\beta_k V_k)\left(\beta_i V_j + \beta_j V_i\right)\right) + a_6(\alpha_k V_k)(\beta_k V_k)\left(\alpha_i\beta_j + \alpha_j\beta_i\right) + a_7 V_i V_j \quad (15)$$

where a_1 to a_7 represent tensor values for a_{11} to a_{55} in matrix 13, and α, β, γ are vectors in the x- and y-axes, and $\gamma = \alpha \times \beta$.

As the geometric symmetries decrease beyond hexagonal and tetragonal cases, it becomes increasingly difficult to build relationships between dispersion and dispersivity using this method. Fel and Bear (2009) also proposed a linear algebraic approach to identify individual components of the dispersivity tensors but did not provide a general methodology to solve these components, nor relate the sensitivity and influence of individual dispersivity tensor terms to principal dispersion values.

Currently the contaminant transport problems in hydrogeology, including numerical models used in legal cases, are primarily based on the Gaussian model of dispersion with an isotropic dispersivity tensor. However, isotopic symmetry is an insufficient model of dispersion, more complicated asymmetric models are needed, and can be justified by the geology. Bear, who first recognized that dispersivity tensor is 4^{th} rank, stated over 50 years ago that dispersivity is not isotropic and needs to be further explored (Bear, 1972). In this study, a different approach is proposed to study the form of the dispersivity tensor and resultant principal dispersion values for a broader set of axial symmetries. Specifically, a framework is presented that is applicable for any crystallographic axial symmetry, and connects diagonal components of the dispersion tensor to independent terms of the dispersivity tensor. Sensitivity and contribution of each individual dispersivity term on the resultant dispersion tensor is assessed, and synthetic particle plumes generated using lattice networks are used to parameterize the dispersivity tensor for hexagonal-tetragonal and orthorhombic symmetries. Visualizations of resultant two-dimensional and three-dimensional Gaussian densities for the axial symmetries are also presented.

CHAPTER 2

BUILDING RELATIONSHIPS AMONG DISPERSION, DISPERSIVITY AND VELOCITY

In this chapter, relationships between dispersion, dispersivity, and the velocity tensors are defined. The analyses performed are intentionally simplified by focusing on how changes in dispersivity affect dispersion. Tensorial forms of dispersivity are provided for isotropic, hexagonal, tetragonal cases in matrices 10, 12, and 13, respectively. For orthorhombic, monoclinic, and triclinic symmetries, the three-dimensional dispersivity tensor can be expressed as (Sirotin and Shaskolskaia, 1982):

$$a_{pq} \cong a_{ijkl} = \begin{vmatrix} a_{11} & a_{12} & a_{13} & 0 & 0 & 0 \\ a_{21} & a_{22} & a_{23} & 0 & 0 & 0 \\ a_{31} & a_{32} & a_{33} & 0 & 0 & 0 \\ 0 & 0 & 0 & a_{44} & 0 & 0 \\ 0 & 0 & 0 & 0 & a_{55} & 0 \\ 0 & 0 & 0 & 0 & 0 & a_{66} \end{vmatrix}. \tag{16}$$

$$a_{pq} \cong a_{ijkl} = \begin{vmatrix} a_{11} & a_{12} & a_{13} & 0 & 0 & a_{16} \\ a_{21} & a_{22} & a_{23} & 0 & 0 & a_{26} \\ a_{31} & a_{32} & a_{33} & 0 & 0 & a_{36} \\ 0 & 0 & 0 & a_{44} & a_{45} & 0 \\ 0 & 0 & 0 & a_{54} & a_{55} & 0 \\ a_{61} & a_{62} & a_{63} & 0 & 0 & a_{66} \end{vmatrix}, \tag{17}$$

$$a_{pq} \cong a_{ijkl} = \begin{vmatrix} a_{11} & a_{12} & a_{13} & a_{14} & a_{15} & a_{16} \\ a_{21} & a_{22} & a_{23} & a_{24} & a_{25} & a_{26} \\ a_{31} & a_{32} & a_{33} & a_{34} & a_{35} & a_{36} \\ a_{41} & a_{42} & a_{43} & a_{44} & a_{45} & a_{46} \\ a_{51} & a_{52} & a_{53} & a_{54} & a_{55} & a_{56} \\ a_{61} & a_{62} & a_{63} & a_{64} & a_{65} & a_{66} \end{vmatrix}. \tag{18}$$

The number of non-zero elements for orthorhombic (matrix 16), monoclinic (matrix 17), and triclinic (matrix 18) cases are 12, 20, and 36, respectively. Triclinic is the most general case; all other symmetry cases can be considered as a special case of triclinic.

Fig. 1 provides a summary example of crystal symmetries. Sides *a*, *b* and *c* correspond to *x*-, *y*- and *z*-axes in a Cartesian coordinate system, and α, β, γ are interaxial angles. The primary differences between the crystal systems are the edge lengths and the interaxial angles. For instance, the difference between hexagonal, tetragonal, and orthorhombic system is the *X*-*Y* plane. The shape of the *X*-*Y* plane in hexagonal, tetragonal, and orthorhombic system is rhombus, square, and rectangle, respectively. Also note that orthorhombic and monoclinic systems are equivalent if restricted to the *X*-*Y* plane. Plume growth according to dispersivity tensors defined for each of these crystallographic systems has different characteristics. This will be addressed in the next chapters.

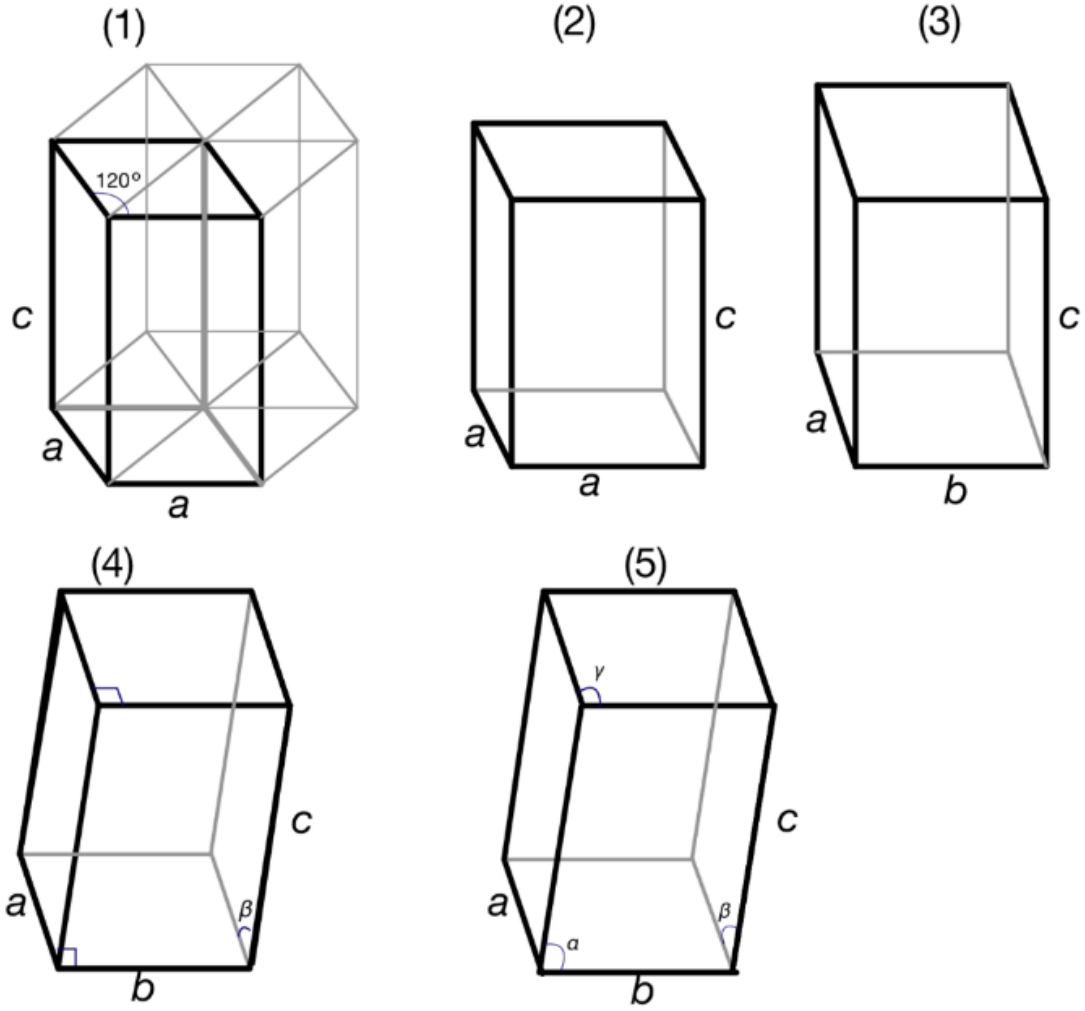

Figure. 1: Example of crystal system:(1) hexagonal system (2) tetragonal system (3) orthorhombic system (4) monoclinic system (5) triclinic system. Notice that a, b and c are edge lengths, and α, β and γ are interaxial angles.

2.1 Prerequisites

Eq. 3 provides a basis for relating dispersion, dispersivity, and velocity. From this point on, the notation used to denote the dispersion tensor is simplified to $D_1 = D_{11}$, $D_2 = D_{22}$, $D_3 = D_{33}$, $D_4 = D_{12}$, $D_5 = D_{23}$, $D_6 = D_{13}$, and the 2nd rank dyadic velocity tensor is represented as a one-dimension column vector:

$$V_k V_l = \begin{vmatrix} V_1 \\ V_1 \\ V_2 \\ V_2 \\ V_3 \\ V_3 \end{vmatrix}. \tag{19}$$

Expressions in three-dimensions for the isotropic, hexagonal, tetragonal, and orthorhombic symmetries are provided below.

For the isotropic case, D_{ij} can be expressed as:

$$|v|D_{ij} = |v| \begin{vmatrix} D_1 \\ D_2 \\ D_3 \\ D_4 \\ D_5 \\ D_6 \end{vmatrix} =$$

$$\begin{vmatrix} a_{11} & a_{12} & a_{12} & 0 & 0 & 0 \\ a_{12} & a_{11} & a_{12} & 0 & 0 & 0 \\ a_{12} & a_{12} & a_{11} & 0 & 0 & 0 \\ 0 & 0 & 0 & \frac{1}{2}(a_{11} - a_{12}) & 0 & 0 \\ 0 & 0 & 0 & 0 & \frac{1}{2}(a_{11} - a_{12}) & 0 \\ 0 & 0 & 0 & 0 & 0 & \frac{1}{2}(a_{11} - a_{12}) \end{vmatrix} \times \begin{vmatrix} V_1 \\ V_1 \\ V_2 \\ V_2 \\ V_3 \\ V_3 \end{vmatrix} \tag{20}$$

$$\Rightarrow D_{ij} = \begin{vmatrix} a_{11}V_1 + a_{12}V_1 + a_{12}V_2 \\ a_{11}V_1 + a_{12}V_1 + a_{12}V_2 \\ a_{11}V_2 + 2a_{12}V_1 \\ \frac{1}{2}(a_{11} - a_{12})V_2 \\ \frac{1}{2}(a_{11} - a_{12})V_3 \\ \frac{1}{2}(a_{11} - a_{12})V_3 \end{vmatrix} \tag{21}$$

$$\Rightarrow D_{ij} = \begin{vmatrix} a_{11}V_1 + a_{12}V_1 + a_{12}V_2 & \frac{1}{2}(a_{11} - a_{12})V_2 & \frac{1}{2}(a_{11} - a_{12})V_3 \\ \frac{1}{2}(a_{11} - a_{12})V_2 & a_{11}V_1 + a_{12}V_1 + a_{12}V_2 & \frac{1}{2}(a_{11} - a_{12})V_3 \\ \frac{1}{2}(a_{11} - a_{12})V_3 & \frac{1}{2}(a_{11} - a_{12})V_3 & a_{11}V_2 + 2a_{12}V_1 \end{vmatrix} \tag{22}$$

where $|v|$ is the magnitude of v. Using the same steps used in Eqs. 20, 21 and 22, D_{ij} for hexagonal, tetragonal, and orthorhombic symmetries are expressed as:

$$D_{ij} = \begin{vmatrix} a_{11}V_1 + a_{12}V_1 + a_{12}V_2 & a_{44}V_2 & \frac{1}{2}(a_{11} - a_{12})V_3 \\ a_{44}V_2 & a_{11}V_1 + a_{12}V_1 + a_{12}V_2 & a_{44}V_3 \\ \frac{1}{2}(a_{11} - a_{12})V_3 & a_{44}V_3 & 2a_{31}V_1 + a_{33}V_2 \end{vmatrix}, \quad (23)$$

$$D_{ij} = \begin{vmatrix} a_{11}V_1 + a_{12}V_1 + a_{13}V_2 & a_{44}V_2 & a_{55}V_3 \\ a_{44}V_2 & a_{11}V_1 + a_{12}V_1 + a_{13}V_2 & a_{44}V_3 \\ a_{55}V_3 & a_{44}V_3 & 2a_{31}V_1 + a_{33}V_2 \end{vmatrix}, \quad (24)$$

and

$$D_{ij} = \begin{vmatrix} a_{11}V_1 + a_{12}V_1 + a_{13}V_2 & a_{44}V_2 & a_{66}V_3 \\ a_{44}V_2 & a_{21}V_1 + a_{22}V_1 + a_{23}V_2 & a_{55}V_3 \\ a_{66}V_3 & a_{55}V_3 & a_{31}V_1 + a_{32}V_1 + a_{33}V_2 \end{vmatrix}. \quad (25)$$

If the problem is simplified to two-dimensions to limit the number of dispersivity terms to 16, the most general expression for the dispersivity tensor for triclinic symmetry is:

$$a_{ijkl} = \begin{vmatrix} a_{11} & a_{12} & a_{13} & a_{14} \\ a_{21} & a_{22} & a_{23} & a_{24} \\ a_{31} & a_{32} & a_{33} & a_{34} \\ a_{41} & a_{42} & a_{43} & a_{44} \end{vmatrix}. \quad (26)$$

Similarly, dispersion for the two-dimensional triclinic case can be expressed as:

$$D_{ij} = \begin{vmatrix} a_{11}V_1 + a_{12}V_1 + a_{13}V_2 + a_{14}V_2 & a_{31}V_1 + a_{32}V_1 + a_{33}V_2 + a_{34}V_2 \\ a_{41}V_1 + a_{42}V_1 + a_{43}V_2 + a_{44}V_2 & a_{21}V_1 + a_{22}V_1 + a_{23}V_2 + a_{24}V_2 \end{vmatrix}. \quad (27)$$

2.2 Expressions and Validations

The expression of D_{ij} in three-dimensions is rewritten as $D_{ij} = \begin{vmatrix} D_1 & D_4 & D_6 \\ D_4 & D_2 & D_5 \\ D_6 & D_5 & D_3 \end{vmatrix}$ and then aligned along principal directions of a Euclidean coordinate system to diagonalize the matrix, such that $D_{ij} = \begin{vmatrix} D_{xx} & 0 & 0 \\ 0 & D_{yy} & 0 \\ 0 & 0 & D_{zz} \end{vmatrix}$. A two-dimensional case is used to simplify the triclinic symmetry, where $D_{ij} = \begin{vmatrix} D_{xx} & 0 \\ 0 & D_{yy} \end{vmatrix}$ along principal directions. Relationships between dispersion, dispersivity, and velocity for any symmetry case can be analytically derived using general expressions:

$$\begin{aligned} D_{xx} &= \alpha a_{xx} V_1 + \beta a_{yy} V_1 + \gamma a_{zz} V_1 \\ D_{yy} &= \alpha a_{xx} V_2 + \beta a_{yy} V_2 + \gamma a_{zz} V_2 \\ D_{zz} &= \alpha a_{xx} V_3 + \beta a_{yy} V_3 + \gamma a_{zz} V_3 \end{aligned} \tag{28}$$

where α, β, γ are coefficients.

Validation of the analytical derivations for each of the symmetries consists of the following procedure:

1. Calculate $D_{ij} = a_{ijkl} \frac{V_k V_l}{v}$ directly. Mark the result as D_{ij1}.
2. Calculate D_{ij} from the derived analytical expressions. Mark the result as D_{ij2}.
3. Subtract D_{ij1} from D_{ij2}. The difference between the two terms should closely approach or equal 0 if the derived expressions are correct.

2.3 Calculation

Dispersivity is a parameter that describes the characteristic spreading of a solute within a porous medium. Our purpose in studying the dispersivity tensor is to understand the connection between a_{ijkl} and D_{ij} for each symmetry case and evaluate the overall contribution of each dispersivity term. The full tensor form of D_{ij} is first derived and eigenvalues are used to solve for the diagonal components $D_{11,}$ D_{22} and D_{33}. Using a Euclidean coordinate system, these diagonal components can be expressed D_{xx}, D_{yy}, and D_{zz}.

2.3.1 Two-Dimensional General Case (Triclinic)

Triclinic is the most general case with all 36 non-zero terms in three-dimensions. In the two-dimensional case, the number of unknown values is reduced to 16, which greatly simplifies the calculation.

D_{ij} is diagonalized by taking the eigenvalues of matrix 27 according to the following steps:

$$\begin{vmatrix} \lambda - (a_{11}V_1 + a_{12}V_1 + a_{13}V_2 + a_{14}V_2) & -a_{31}V_1 - a_{32}V_1 - a_{33}V_2 - a_{34}V_2 \\ -a_{41}V_1 - a_{42}V_1 - a_{43}V_2 - a_{44}V_2 & \lambda - (a_{21}V_1 + a_{22}V_1 + a_{23}V_2 + a_{24}V_2) \end{vmatrix} \quad (29)$$

$$\Rightarrow (\lambda - (a_{11}V_1 + a_{12}V_1 + a_{13}V_2 + a_{14}V_2))(\lambda - (a_{21}V_1 + a_{22}V_1 + a_{23}V_2 + a_{24}V_2)) - (a_{31}V_1 + a_{32}V_1 + a_{33}V_2 + a_{34}V_2)(a_{41}V_1 + a_{42}V_1 + a_{43}V_2 + a_{44}V_2) = 0 \quad (30)$$

The two roots of this equation λ_1 and λ_2 are the dispersion values.

$$D_{ij} = \begin{vmatrix} \lambda_1 & 0 \\ 0 & \lambda_2 \end{vmatrix}. \quad (31)$$

and can be solved according to the relationships provided in Appendix A.

2.3.2 Hexagonal

From matrix 23, let:

$$\begin{cases} a = a_{11}V_1 + a_{12}V_1 + a_{12}V_2 \\ b = 2a_{31}V_1 + a_{33}V_2 \\ c = a_{44}V_2 \\ d = a_{44}V_3 \\ e = \frac{1}{2}(a_{11} - a_{12})V_3 \end{cases}. \tag{32}$$

Then matrix 23 becomes:

$$D_{ij} = \begin{vmatrix} a & c & e \\ c & a & d \\ e & d & b \end{vmatrix}. \tag{33}$$

Finding eigenvalues for D_{ij}:

$$\begin{vmatrix} \lambda - a & -c & -e \\ -c & \lambda - a & -d \\ -e & -d & \lambda - b \end{vmatrix} = 0 \tag{34}$$

$$\Rightarrow (\lambda - a)(\lambda - a)(\lambda - b) - c^2(\lambda - b) - d^2(\lambda - a) - e^2(\lambda - a) = 0. \tag{35}$$

The three roots of this equation λ_1, λ_2 and λ_3 are the dispersion values.

$$D_{ij} = \begin{vmatrix} \lambda_1 & 0 & 0 \\ 0 & \lambda_2 & 0 \\ 0 & 0 & \lambda_3 \end{vmatrix}. \tag{36}$$

and can be solved according to the relationships provided in Appendix A.

2.3.3 Tetragonal

From matrix 24, let:

$$\begin{cases} a = a_{11}V_1 + a_{12}V_1 + a_{13}V_2 \\ b = 2a_{31}V_1 + a_{33}V_2 \\ c = a_{44}V_2 \\ d = a_{44}V_3 \\ e = a_{55}V_3 \end{cases} . \quad (37)$$

Similarly, solving for equation:

$$(\lambda - a)(\lambda - a)(\lambda - b) - c^2(\lambda - b) - d^2(\lambda - a) - e^2(\lambda - a) = 0 \quad (38)$$

Results are presented in Appendix A.

2.3.4 Orthorhombic

From matrix 25, let:

$$\begin{cases} a = a_{11}V_1 + a_{12}V_1 + a_{13}V_2 \\ b = a_{21}V_1 + a_{22}V_1 + a_{23}V_2 \\ c = a_{31}V_1 + a_{32}V_1 + a_{33}V_2 \\ d = a_{44}V_2 \\ e = a_{55}V_3 \\ f = a_{66}V_3 \end{cases} \quad (39)$$

Similarly, solving for equation:

$$(\lambda - a)(\lambda - b)(\lambda - c) - 2def - f^2(\lambda - b) - d^2(\lambda - c) - e^2(\lambda - a) = 0 \quad (40)$$

Results are presented in Appendix A.

The expressions derived for the hexagonal, tetragonal, orthorhombic, and triclinic symmetries are validated according to the methodology in Chapter 2.2. Appendix A also provides an example of the validation of the derivation for the two-dimensional general triclinic case.

CHAPTER 3

SENSITIVITY ANALYSIS

In one-dimension, dispersion is a linear product of dispersivity and velocity, where $D = a \cdot v$ and all variables are scalar. In higher dimensions, relations between these variables are less clear: dispersion and velocity are both 2^{nd} rank tensors, and dispersivity is a 4^{th} rank tensor that can have up to 36 independent, non-zero terms. Each non-zero dispersivity term, or groups of dispersivity terms according to tensor symmetry, should have distinct contributions to the principal components (diagonal values) of the dispersion tensor. To determine the influence of individual terms of dispersivity on principal components of dispersion, a sensitivity analysis is performed for hexagonal, tetragonal, and orthorhombic symmetries. The impact of the velocity tensor is generalized by applying the condition $v = 1$ to facilitate direct study of the influence of a_{ijkl} on D_{ij}. The x-axis is manually set to represent the main plume transport direction such that D_{xx} is the dominant dispersion term for all symmetries.

3.1 Hexagonal, Tetragonal, and Orthorhombic Symmetry

Hexagonal, tetragonal, and orthorhombic systems have 6, 7, and 12 independent terms, respectively. Each of these terms must have some impact on the resultant dispersion tensor, yet defining the overall contribution is challenging to understand and cannot be determined from visual methods. A sensitivity analysis is performed where the dispersivity term of interest is allowed to vary over the interval $a \in [0,10]$, while all other dispersivity terms are

assigned a value of unity. All values should satisfy the constraint conditions in matrix 4. The corresponding principal values of the dispersion tensor (D_{xx}, D_{yy}, D_{zz}) are then computed as eigenvalues. The relative influence of each dispersivity term in the hexagonal symmetry is shown in Fig. 2a, 2b and 2c. The relative influence of each dispersivity term in the tetragonal symmetry is shown in Fig. 2d, 2e and 2f. Fig. 2g, 2h and 2i illustrate the relative influence of each dispersivity term in the orthorhombic symmetry. The impact of each single dispersivity term is classified as major, minor, no impact, or limited in Table 1.

Figure. 2: Sensitivity analysis of the principal components of the dispersion tensor to dispersivity tensor values for hexagonal a - c, tetragonal d - f, and orthorhombic g - i symmetries.

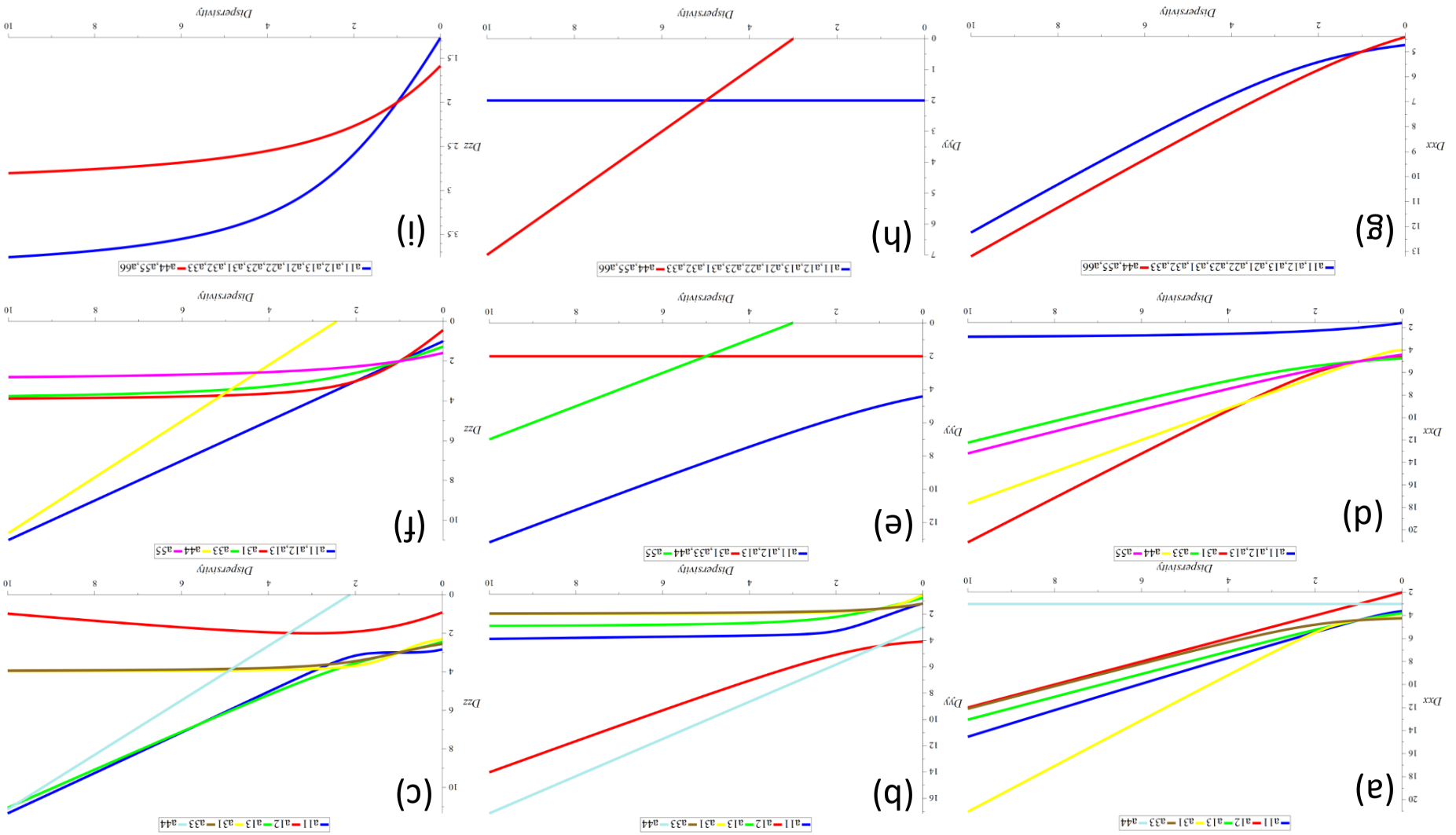

Table 1: Impact of each single dispersivity variable to dispersion value for (1a) hexagonal symmetry, (1b) tetragonal symmetry, and (1c) orthorhombic symmetry.

(a)

	Impact			
Dispersion	Major	Minor	None	Converge to Limits
D_{xx}	a_{11}	a_{12}, a_{13}, a_{31}, a_{33}	a_{44}	N/A
D_{yy}	a_{44}	a_{12}	N/A	a_{11}, a_{13}, a_{31}, a_{33}
D_{zz}	a_{11}, a_{13}, a_{44}	a_{12}	N/A	a_{31}, a_{33}

(b)

	Impact			
Dispersion	Major	Minor	None	Converge to Limits
D_{xx}	a_{31}, a_{44}	a_{33}, a_{55}	N/A	a_{11}, a_{12}, a_{13}
D_{yy}	a_{11}, a_{12}, a_{13}	a_{55}	a_{31}, a_{33}, a_{44}	N/A
D_{zz}	a_{11}, a_{12}, a_{13}, a_{44}	N/A	N/A	a_{31}, a_{33}, a_{55}

(c)

	Impact			
Dispersion	Major	Minor	None	Converge to Limits
D_{xx}	Major and minor changes with different interval setting.			
			a_{11}, a_{12}, a_{13}, a_{21} a_{22}, a_{23}, a_{31}, a_{32}, a_{33}	
D_{yy}	a_{44}, a_{55}, a_{66}	N/A		N/A
D_{zz}	N/A	N/A	N/A	All

In the hexagonal system, 4 out of 6 terms ($a_{11,}$ a_{12}, a_{13}, a_{31}) exert major influence on D_{xx}, a_{33} exerts a minor influence on D_{xx}, and a_{44} has no impact on D_{xx}. Both a_{12} and a_{44} exert major influence on D_{yy}, and D_{yy} asymptotically converges to a limit when a_{11}, a_{13}, a_{31}, a_{33} are sufficiently large. For D_{zz}, a_{11}, a_{12}, a_{13} and a_{44} are the major terms. Similar to the results observed for D_{yy}, D_{zz} converges to a limit when a_{31} and a_{33} are sufficiently large. These trends indicate that plume growth according to hexagonal symmetry is concentrated along a dominant axis (x-axis), and restricted along the y- and z-axes. When the value of a_{13} is greater

than $\frac{3\sqrt{2}}{2}$ (due to the constraint conditions), D_{zz} is proportional to a_{13}. This trend is dissimilar to the isotropic symmetry case where dispersivity and dispersion are always linearly proportional.

Values assigned to a_{31} and a_{44} in the tetragonal system exert major influence on D_{xx}, while a_{33} and a_{55} exert only minor influence. Unlike the hexagonal system, D_{xx} converges to an upper limit when a_{11}, a_{12}, a_{13} are sufficiently large. Terms a_{11}, a_{12}, a_{13} have major impact on D_{yy}, a_{55} has minor impact, and a_{31}, a_{33}, a_{44} have no impact. Terms a_{11}, a_{12}, a_{13}, a_{44} exert major influences on D_{zz}. Similar to the hexagonal system, D_{zz} converges to an upper limit when a_{31}, a_{33}, a_{35} are sufficiently large. The influence of the 12 dispersivity terms on D_{xx}, D_{yy}, and D_{zz} can all be classified into two groups for the orthorhombic system: a_{11}, a_{12}, a_{13}, a_{21}, a_{22}, a_{23}, a_{31}, a_{32}, a_{33}, and a_{44}, a_{55}, a_{66}. In each group, all terms have the same contribution to dispersion, whereas the impact of different groups vary according to the interval tested. Over the interval (0,1), a_{11}, a_{12}, a_{13}, a_{21}, a_{22}, a_{23}, a_{31}, a_{32}, a_{33} exert significant influence on D_{xx} with only minor contributions from a_{44}, a_{55}, a_{66}. When the interval is greater than 1, a_{44}, a_{55}, a_{66} more significantly affect D_{xx} than a_{11}, a_{12}, a_{13}, a_{21}, a_{22}, a_{23}, a_{31}, a_{32}, a_{33}. Only a_{44}, a_{55}, a_{66} affect D_{yy}, with a_{11}, a_{12}, a_{13}, a_{21}, a_{22}, a_{23}, a_{31}, a_{32}, a_{33} having no impact on D_{yy}. For D_{zz}, both groups converge to upper limits when dispersivity variables are sufficiently large.

3.2 Generalization to All Symmetries

To explore reasons why some dispersivity terms: (1) have major, minor, or no impact on dispersion, (2) contribute equally to dispersion, or (3) result in the convergence to a constant when sufficiently large, these symmetries are further examined. For comparison purposes, all symmetries discussed in the paper can be considered as special cases of triclinic

system. In hexagonal, tetragonal, and orthorhombic systems, only 12 out of a possible 36 terms are non-zero. Of these 12 terms, only 6 and 7 terms, respectively, in hexagonal and tetragonal systems are independent due to symmetry relations, e.g., $a_{11} = a_{22}, a_{12} = a_{21}, a_{13} = a_{23}$. For these two symmetries, there is a dependence where some terms influence values of other terms, e.g., a_{11}, a_{12} and a_{13} influence values of a_{22}, a_{21} and a_{23}, respectively.

However, unlike the hexagonal and tetragonal systems, all 12 non-zero terms are independent in an orthorhombic system. For higher symmetries with more axes of rotation (e.g., hexagonal and tetragonal), each term exerts greater influence on dispersion than lower symmetry systems with fewer axes of rotation (e.g., orthorhombic, monoclinic, triclinic) where groups of terms have similar influence.

For instance, changing the value of one term will change at least one additional term among those 12 non-zero terms in the hexagonal and tetragonal system, e.g., changes to a_{13} and a_{23} are interconnected since $a_{13} = a_{23}$. Conversely, in the orthorhombic system, changing the value of a_{13} will not lead to the change of any other variables other than a_{13} itself. This explains why many terms exert a major influence on dispersion in a hexagonal system, while at the same time some terms like a_{33} only exert minor impact to D_{xx}. In this case, a_{33} is the only term in the first defined group that does not pair to any other terms. Using the most general expression (matrix 18):

$$a_{pq} \cong a_{ijkl} = \left|\begin{array}{ccc:ccc} a_{11} & a_{12} & a_{13} & a_{14} & a_{15} & a_{16} \\ a_{21} & a_{22} & a_{23} & a_{24} & a_{25} & a_{26} \\ a_{31} & a_{32} & a_{33} & a_{34} & a_{35} & a_{36} \\ \hdashline a_{41} & a_{42} & a_{43} & a_{44} & a_{45} & a_{46} \\ a_{51} & a_{52} & a_{53} & a_{54} & a_{55} & a_{56} \\ a_{61} & a_{62} & a_{63} & a_{64} & a_{65} & a_{66} \end{array}\right|$$

individual dispersivity terms can be organized into four groups, where group 1 $= \begin{cases} p = 1,2,3 \\ q = 1,2,3 \end{cases}$, group 2 $= \begin{cases} p = 1,2,3 \\ q = 4,5,6 \end{cases}$, group 3$= \begin{cases} p = 4,5,6 \\ q = 1,2,3 \end{cases}$, and group 4 $= \begin{cases} p = 4,5,6 \\ q = 4,5,6 \end{cases}$. Note that a_{44} is

located in a different group other than a_{11}, a_{12}, a_{13}, a_{31} and a_{33} in the hexagonal system (Matrix 12). This organization explains why a_{44} is the only variable that exerts a zero impact on D_{xx}, yet is the only variable that exerts a major influence on D_{yy}.

In a broader sense, the combination of the dependence structure and grouping are responsible for the impact of the dispersivity terms on dispersion. Term location within the tensor first decides if a group of variables will influence dispersion, and tensor dependence (based on individual symmetries) determines which terms will have either major or minor influence on dispersion. For instance, only terms in group 1 can influence D_{xx} in the hexagonal system. Among those terms in group 1, a_{33} is the only independent term, and consequently exerts a minor impact on D_{xx}. The other terms in group 1 (a_{11}, a_{12}, a_{13} and a_{31}) all exert a similar major influence on D_{xx}. Similarly, only terms in group 4 can influence D_{yy}, as a_{12} and a_{44} (note that $a_{66} = (a_{11} - a_{12})/2$, but a_{11} did not influence D_{yy}) are the two terms that exert major influence on D_{yy}. Both groups 1 and 4 influence D_{zz}. Due to the restriction of plume growth along the minor axes, D_{zz} converges to a constant value when a_{12}, a_{31} and a_{33} are sufficiently large.

Since all 12 non-zero terms in the orthorhombic system are independent, all terms in the same group have the same influence on dispersion. However, the relative influence of each dispersivity term on D_{xx}, D_{yy}, and D_{zz} depends on group location. Both group 1 (a_{11}, a_{12}, a_{13}, a_{21}, a_{22}, a_{23}, a_{31}, a_{32}, a_{33}) and group 4 (a_{44}, a_{55}, a_{66}) contribute to D_{xx}, whereas group 4 exclusively controls D_{yy}.

The primary difference between hexagonal and tetragonal symmetries is that a_{55} in the tetragonal symmetry does not equal $(a_{11} - a_{12})/2$ (Matrices 12 and 13). Both groups 1 (a_{11}, a_{12}, a_{13}, a_{31} and a_{33}) and 4 (a_{44} and a_{55}) control D_{xx}. Here a_{33} and a_{55} are the only two independent variables in the tetragonal system and thus they exert only minor impacts on D_{xx}. In the most

general case of triclinic, all 36 terms are non-zero and independent. Due to the lack of dependence, all terms within the same group contribute equally to dispersion. Thus, as symmetries become more generalized and less ordered, dispersion is not controlled by individual dispersivity terms, but rather by the contributions of each of the four groups.

Lastly, the impact of dispersivity terms on D_{zz} warrants further explanation. Transitions from higher (isotropic) to lower (orthorhombic) symmetries, lead to plume growth that becomes more focused along a single major direction and restricted along the other two minor directions. This is shown in Fig. 2c, 2f, 2i, which describe dispersion along the *z*-axis. In Fig. 2c, only 2 of 6 dispersion values which correspond to dispersivity variables converge to the constants. In Fig. 2f, 3 of the 7 dispersion values which correspond to dispersivity converge to the constants. This means that only a subset of dispersivity terms in the hexagonal and tetragonal symmetries lead to principal dispersion coefficients that reach asymptotic limits, and consequently plume growth along the *z*-axis is not fully restricted. However, in Fig. 2i, all 12 dispersion values which correspond to dispersivity reach asymptotic limits, restricting plume growth along the *z*-axis. These restrictions on plume growth do not exist in monoclinic and triclinic system. These details will become clearer in the next chapter.

CHAPTER 4

MULTIVARIATE GAUSSIAN VISUALIZATION AND TENSOR APPLICATION

Resultant two-dimensional and three-dimensional Gaussian densities for each of the axial symmetries represent the transport solution of a non-reactive contaminant in a groundwater flow system (as described in Eq. 1) given a Dirac delta impulse representing an instantaneous, point injection into an initially clean aquifer. Fig. 3 provides a useful illustration of a three-dimensional plume resulting from an instantaneous injection at point (x_0, y_0, z_0) with concentration C_0. The plume migrates to point (ξ, η, ψ) after a certain time. The probability of solute concentration at a certain point follows a trivariate Gaussian distribution with the following expression (Bear, 1961):

$$C(x,y,z;x',y',z') = \frac{C_0}{2\sigma_x\sigma_y\sigma_z\sqrt{2\pi}} \cdot exp\left(-\frac{(x-x')^2}{2\sigma_x^2} - \frac{(y-y')^2}{2\sigma_y^2} - \frac{(z-z')^2}{2\sigma_z^2}\right), \quad (41)$$

where:

$$\sigma_x = \sqrt{D_{xx}}, \sigma_y = \sqrt{D_{yy}}, \sigma_z = \sqrt{D_{zz}}\,.$$

Eq. 41 is applicable for either plotting resultant plumes or calculating concentrations at any point.

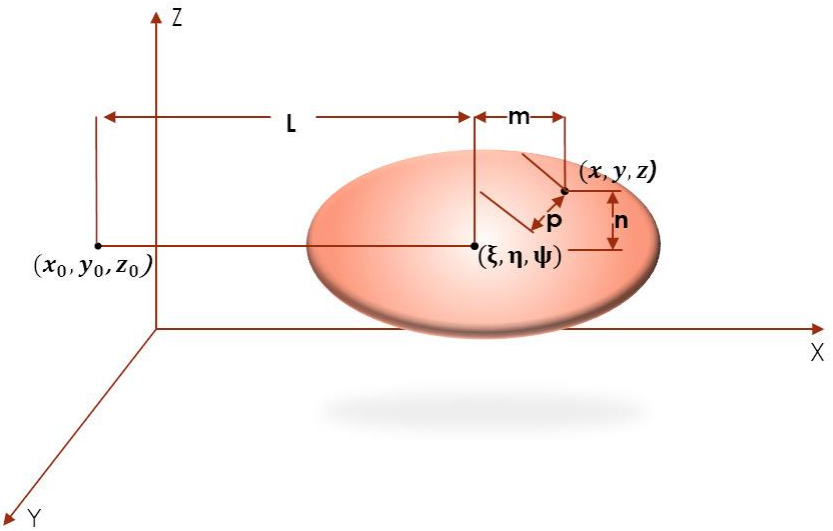

Figure. 3: Three-dimensional plume (multi-Gaussian density) after some elapsed time resulting from an instantaneous point injection of a conservative solute. Point (x, y, z) are the coordinates of the point at a certain moment, and *m p* and *n* are the distance of the point (x, y, z) to the plume center (ξ, η, ψ), respectively, and *L* is the mean displacement of the center of plume mass.

4.1 Plume Visualization for Axial Symmetries

To date, field-scale contaminant plumes have not been used to define dispersivity terms for the symmetry cases studied. Alternatively, multi-Gussian densities are illustrated for each of the symmetry cases by randomly assigning dispersivity terms within the interval [0,10] (must satisfy constraint conditions in matrix 4), computing D_{ij}, and plotting the corresponding density using Eq. 41. To control the variables, the same elements in different symmetries (e.g., a_{11}, a_{12}, a_{13}, a_{31}, a_{33} and a_{44} in hexagonal and tetragonal symmetry, matrix 12 and 13) were assigned the same values. The plume is centered at (0, 0, 0) for convenience, and velocity is simplified according to Eq. 19. These steps are executed using the Maple software suite, although the procedure itself is software independent.

4.1.1 Isotropic

An isotropic dispersivity tensor is defined in accordance with matrix 10:

$$a_{ijkl} = \begin{vmatrix} 2 & 1 & 1 & 0 & 0 & 0 \\ 1 & 2 & 1 & 0 & 0 & 0 \\ 1 & 1 & 2 & 0 & 0 & 0 \\ 0 & 0 & 0 & 0.5 & 0 & 0 \\ 0 & 0 & 0 & 0 & 0.5 & 0 \\ 0 & 0 & 0 & 0 & 0 & 0.5 \end{vmatrix} \tag{42}$$

and generates dispersion tensor:

$$D_{ij} = \begin{vmatrix} 3.5 & 0 & 0 \\ 0 & 5 & 0 \\ 0 & 0 & 3.5 \end{vmatrix}. \tag{43}$$

4.1.2 Hexagonal

Similarly, a hexagonal dispersivity tensor is defined in accordance with matrix 12:

$$a_{ijkl} = \begin{vmatrix} 4 & 1 & 3 & 0 & 0 & 0 \\ 1 & 4 & 3 & 0 & 0 & 0 \\ 2 & 2 & 5 & 0 & 0 & 0 \\ 0 & 0 & 0 & 3 & 0 & 0 \\ 0 & 0 & 0 & 0 & 3 & 0 \\ 0 & 0 & 0 & 0 & 0 & 1.5 \end{vmatrix}. \tag{44}$$

and generates dispersion tensor:

$$D_{ij} = \begin{vmatrix} 13.38 & 0 & 0 \\ 0 & 7.02 & 0 \\ 0 & 0 & 4.60 \end{vmatrix}. \tag{45}$$

4.1.3 Tetragonal

Like previous examples, a tetragonal dispersivity tensor is defined in accordance with matrix 13:

$$a_{ijkl} = \begin{vmatrix} 4 & 1 & 3 & 0 & 0 & 0 \\ 1 & 4 & 3 & 0 & 0 & 0 \\ 2 & 2 & 6 & 0 & 0 & 0 \\ 0 & 0 & 0 & 3 & 0 & 0 \\ 0 & 0 & 0 & 0 & 3 & 0 \\ 0 & 0 & 0 & 0 & 0 & 6 \end{vmatrix}. \quad (46)$$

and generates dispersion tensor:

$$D_{ij} = \begin{vmatrix} 16.61 & 0 & 0 \\ 0 & 2.47 & 0 \\ 0 & 0 & 5.92 \end{vmatrix}. \quad (47)$$

4.1.4 Orthorhombic

An orthorhombic dispersivity tensor is defined in accordance with matrix 16:

$$a_{ijkl} = \begin{vmatrix} 2 & 3.5 & 6 & 0 & 0 & 0 \\ 2.5 & 1.5 & 5.5 & 0 & 0 & 0 \\ 0.5 & 3 & 7 & 0 & 0 & 0 \\ 0 & 0 & 0 & 8 & 0 & 0 \\ 0 & 0 & 0 & 0 & 9 & 0 \\ 0 & 0 & 0 & 0 & 0 & 10 \end{vmatrix}. \quad (48)$$

$$D_{ij} = \begin{vmatrix} 28.58 & 0 & 0 \\ 0 & 2.44 & 0 \\ 0 & 0 & 0.48 \end{vmatrix}. \quad (49)$$

4.1.5 Monoclinic

A monoclinic dispersivity tensor is defined in accordance with matrix 17:

$$a_{ijkl} = \begin{vmatrix} 8.9 & 3.2 & 5.9 & 0 & 0 & 2 \\ 8.5 & 8 & 0.2 & 0 & 0 & 7.1 \\ 9.3 & 1.9 & 3 & 0 & 0 & 2.3 \\ 0 & 0 & 0 & 7 & 6.7 & 0 \\ 0 & 0 & 0 & 7.5 & 5.1 & 0 \\ 3.3 & 1.8 & 4.3 & 0 & 0 & 1.2 \end{vmatrix} \quad (50)$$

$$D_{ij} = \begin{vmatrix} 45.18 & 0 & 0 \\ 0 & 8.12 & 0 \\ 0 & 0 & 6.99 \end{vmatrix}. \quad (51)$$

4.1.6 Triclinic

A triclinic dispersivity tensor is defined in accordance with matrix 18:

$$a_{ijkl} = \begin{vmatrix} 8.9 & 3.2 & 5.9 & 2.4 & 5.8 & 2 \\ 8.5 & 8 & 0.2 & 5.2 & 3.7 & 7.1 \\ 9.3 & 1.9 & 3 & 3.5 & 4.4 & 2.3 \\ 0.6 & 2.9 & 0.8 & 7 & 6.7 & 2.1 \\ 2.1 & 4.1 & 0.7 & 7.5 & 5.1 & 5 \\ 3.3 & 1.8 & 4.3 & 1.6 & 0.4 & 1.2 \end{vmatrix} \quad (52)$$

$$D_{ij} = \begin{vmatrix} 67.50 & 0 & 0 \\ 0 & 14.88 & 0 \\ 0 & 0 & 2.92 \end{vmatrix}. \quad (53)$$

Multi-Gaussian densities (plumes) for each set of D_{ij}, are shown as Fig. 4.

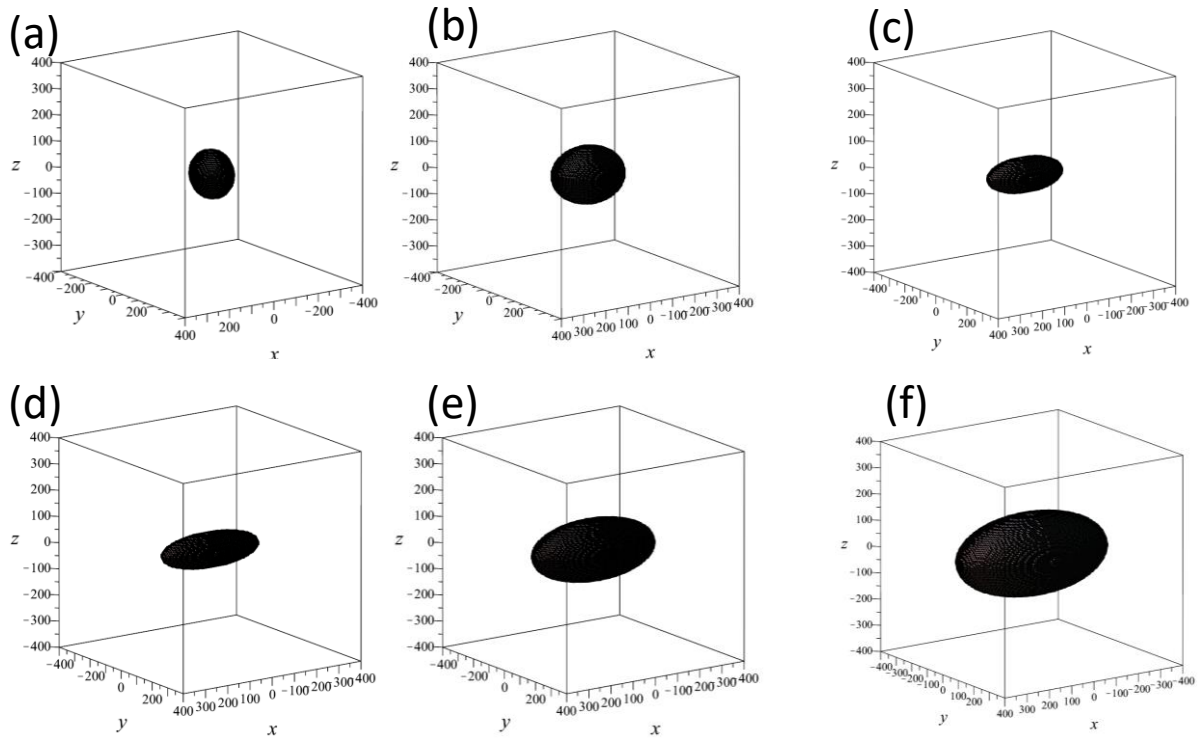

Figure. 4: Shape of the plume in: (a) isotropic system (b) hexagonal system (c) tetragonal system (d) orthorhombic system (e) monoclinic system (f) triclinic system.

4.2 Application of Anisotropic Tensor to Numerical Data

Lattice networks are used to generate synthetic particle plumes for application of the anisotropic dispersivity tensors to geologic analogues. Lattice networks are ideal for testing the full range of symmetries encompassing isotropic, hexagonal, tetragonal, orthorhombic, monoclinic and triclinic symmetries by incorporating specific combinations of grid spacing between nodes (which can be anisotropic), the degree of connection of the line segments to these nodes, and transmissivity (e.g., Sahini et al., 1994). Transmissivity has a base value of 0.0001 m^2/s and may be isotropic or anisotropic. Fluid flow within the lattice bond networks is first simulated using a linear hydraulic gradient that establishes a flow direction from the

top of the model domain to the bottom, followed by advective transport of non-reactive solute particles. These modeling exercises are restricted to two-dimensions for both computational and mathematical (for parameterization of tensor values) simplicity to investigate: (1) resultant plume spreading behavior in the context of different axial symmetries, and (2) possible correlations between characteristics or features of the geologic/lattice systems and the resultant dispersivity and dispersion tensors.

The discrete fracture network methodology described by Parashar and Reeves (2012) is used to solve for fluid flow within the model:

$$Q = -T\frac{dh}{dl} \tag{54}$$

where Q is the volumetric flow through each line segment per unit thickness [L^2/T], T is the transmissivity [L^2/T], h is the hydraulic head at each node [L], and l is distance [L]. For two-dimensional networks, nodes represent intersections between two orthogonal sets of segments (Fig. 5a, 5b, 6a, 6b). Each line segment is assigned a constant transmissivity value and the resultant solute spreading is always a function of network geometry, and anisotropic transmissivity when applied. Flow through the networks is expressed as a linear set of equations to solve for h:

$$Ah = b \tag{55}$$

where A is the coefficient matrix of dimension $n \times n$, n is the number of nodes, and b is a constant head condition applied to the boundary nodes (Parashar and Reeves, 2012). A minimum residual (MINRES) iterative method is used to determine h for all internal nodes given a head solver criterion of 1.0×10^{-6} (Parashar and Reeves, 2012).

A total of 10,000 particles is released into the upgradient portion of the flow field solution and a Lagrangian particle tracking method simulates independent particle trajectories (Reeves et al., 2012). Particle positions are output at selected times for the computation of the

dispersion tensor according to mean plume position and variance in the longitudinal and transverse directions. A Monte Carlo framework is used to generate ensemble particle plumes comprised of results for 100 individual realizations to account for structural uncertainty associated with the network structures.

The lattice network simulations are used to generate plumes with hexagonal-tetragonal (hexagonal and tetragonal symmetries are equivalent in the horizontal direction, e.g., Fig. 1-1 and 1-2) and orthorhombic symmetries. These symmetries are represented by varying node spacing, the degree of line segment connection using a total segment density criterion, and longitudinal and transverse transmissivity. This allows for a systematic evaluation of how directional anisotropy in the lattice networks influences solute spreading and the correspondence to different axial symmetries.

The horizontal cross-section of a hexagonal/tetragonal symmetry along the *x-y* plane is a rhombus. To simulate solute transport consistent with a rhombus geometry, a 1m × 1m grid spacing is applied to the longitudinal and transverse directions (Table 2). To incorporate additional realism and application to geological systems, a spatial density of 0.7 (70% of the nodes are connected to each other) is applied and transmissivity in the longitudinal direction is five times greater than in the transverse direction (Table 2). This system, for example, could represent a moderately connected fracture network where segments in the longitudinal direction are optimally aligned within the stress field for aperture dilation and enhanced flow (Ferrill et al., 1999). Applying a similar concept, orthorhombic symmetries have a rectangular horizontal cross-section along the *x-y* plane. An unequal grid spacing of 2m × 1m along the longitudinal and transverse directions, respectively, is assigned to the lattice networks along with isotropic transmissivity and 0.7 spatial density. The unequal spacing could represent a fracture system with a dominant fracture set direction that has twice the density as the non-dominant set.

Table 2: Parameter sets used to generate lattice networks for hexagonal-tetragonal and orthorhombic systems

Symmetry Type	Domain (m × m)	Grid Spacing (m × m)	Spatial Density	T_l:T_t[a]
Hexagonal-Tetragonal	100 × 100	1 × 1	0.7	5
Orthorhombic	100 × 100	2 × 1	0.7	1

[a] ratio of longitudinal and transverse transmissivity

4.2.1 Hexagonal/Tetragonal

A hexagonal-tetragonal system was generated by using the parameter settings in Table 2. Fig. 5a (Fig 5b is a zoom in view of Fig.5a) shows a representative lattice network. Fig. 5c shows an ensemble lattice network particle plume at time 1.45×10^7 s with longitudinal and transverse variance of 159.23 m^2 and 28.09 m^2, respectively, and Fig. 5d shows the best-fit bivariate Gaussian density. All six non-zero terms in the two-dimensional hexagonal-tetragonal dispersivity tensor are parameterized using the relationship in Eqs. 2, 12, 13:

$$\begin{cases} a_{11} + a_{22} = \frac{\sigma_x^2+\sigma_y^2}{2V_1} \\ a_{33} = \frac{\sigma_y^2-\sigma_x^2}{2V_2} \end{cases}. \tag{56}$$

Setting V_1=1 and V_2=1.5 gives rise to the expression:

$$\begin{cases} a_{11} + a_{22} = 93.66 \\ a_{33} = 43.71 \end{cases}. \tag{57}$$

The sum of a_{11} and a_{12} is constant, and when scaled correctly, any arbitrary value can be input for a_{12}. Setting a_{12} = 30 results in a_{11} = 93.66 – 30 = 63.66, and leads to the full tensor expression:

$$a_{ijkl} = \begin{vmatrix} 63.66 & 30 & 0 & 0 \\ 30 & 63.66 & 0 & 0 \\ 0 & 0 & 43.71 & 0 \\ 0 & 0 & 0 & 43.71 \end{vmatrix}. \quad (58)$$

Using the method in Chapter 4.1, values of a_{ijkl} in matrix 58 were calculated, and the Maple software suite was used to visualize the calculated Multi-Gaussian densities of the generated plumes (Fig. 5d), to be compared with the original data (Fig 5c).

4.2.2 Orthorhombic

Similarly, an orthorhombic system was generated by using the parameter settings in Table 2. The representative lattice network was shown in Fig. 6a (Fig 6b is a zoom in view of Fig.6a). Fig. 6c shows an ensemble lattice network particle plume at time 1.18×10^7 s with longitudinal and transverse variance of 200.40 m^2 and 21.18 m^2, respectively. Fig. 6d shows the best-fit bivariate Gaussian density. All six non-zero terms in the two-dimensional hexagonal-tetragonal dispersivity tensor are parameterized using the relationship in Eqs. 2, 12, 16:

$$\begin{cases} a_{11}V_1 + a_{12}V_1 + a_{21}V_1 + a_{22}V_1 = \sigma_x^2 + \sigma_y^2 \\ (a_{11} + a_{12})(a_{21} + a_{22})V_1^2 - a_{33}a_{44}V_2^2 = \sigma_x^2\sigma_y^2, \end{cases} \quad (59)$$

and:

$$\begin{cases} a_{11}V_1 + a_{12}V_1 \in (\sigma_x^2, \sigma_y^2) \\ a_{21}V_1 + a_{22}V_1 \in (\sigma_x^2, \sigma_y^2), \end{cases} \quad (60)$$

Setting V_1=1 and V_2=1.5, the above expression becomes:

$$\begin{cases} a_{11} + a_{12} + a_{21} + a_{22} = 221.58 \\ (a_{11} + a_{12})(a_{21} + a_{22}) - \frac{9}{4} a_{33} a_{44} V_2^2 = 4244.472 \end{cases} \quad (61)$$

Similarly, setting a_{11} = 10.5, a_{12} = 26.8, a_{21} = 68, a_{22} = 116.28, a_{33} = 24, a_{44} = 48.69. Then,

$$a_{ijkl} = \begin{vmatrix} 10.5 & 26.8 & 0 & 0 \\ 68 & 116.28 & 0 & 0 \\ 0 & 0 & 24 & 0 \\ 0 & 0 & 0 & 48.69 \end{vmatrix}. \quad (62)$$

Calculated bivariate Gaussian densities of the generated plumes (Fig. 6d) can be compared with the original data (Fig 6c).

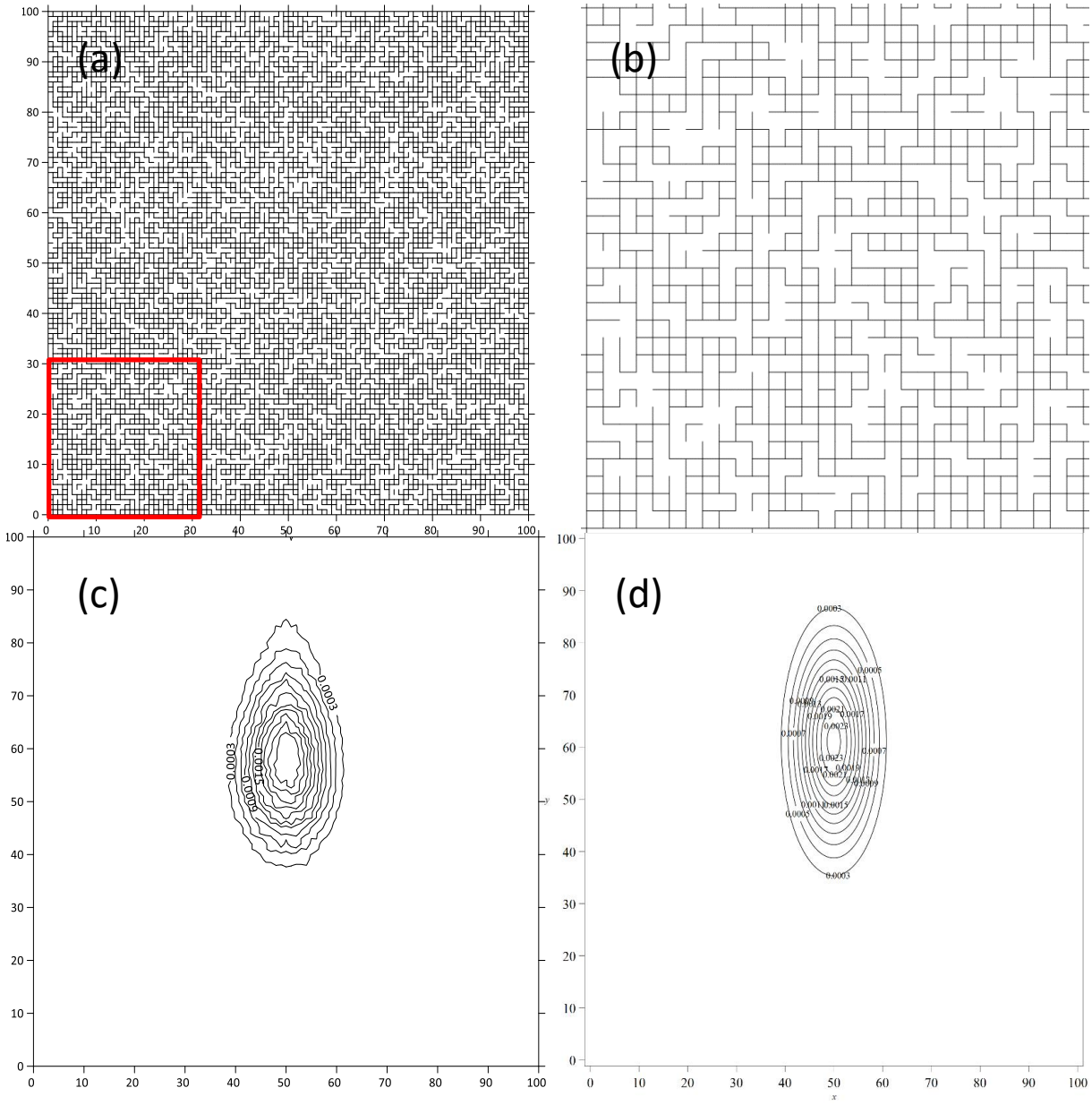

Figure. 5: Numerical simulation of particle transport through hexagonal-tetragonal system where (a) is the lattice network, (b) is a zoomed in view of the selected area in (a), (c) is the bivariate Gaussian density of the synthetic plume, and (d) is the best-fit bivariate Gaussian density.

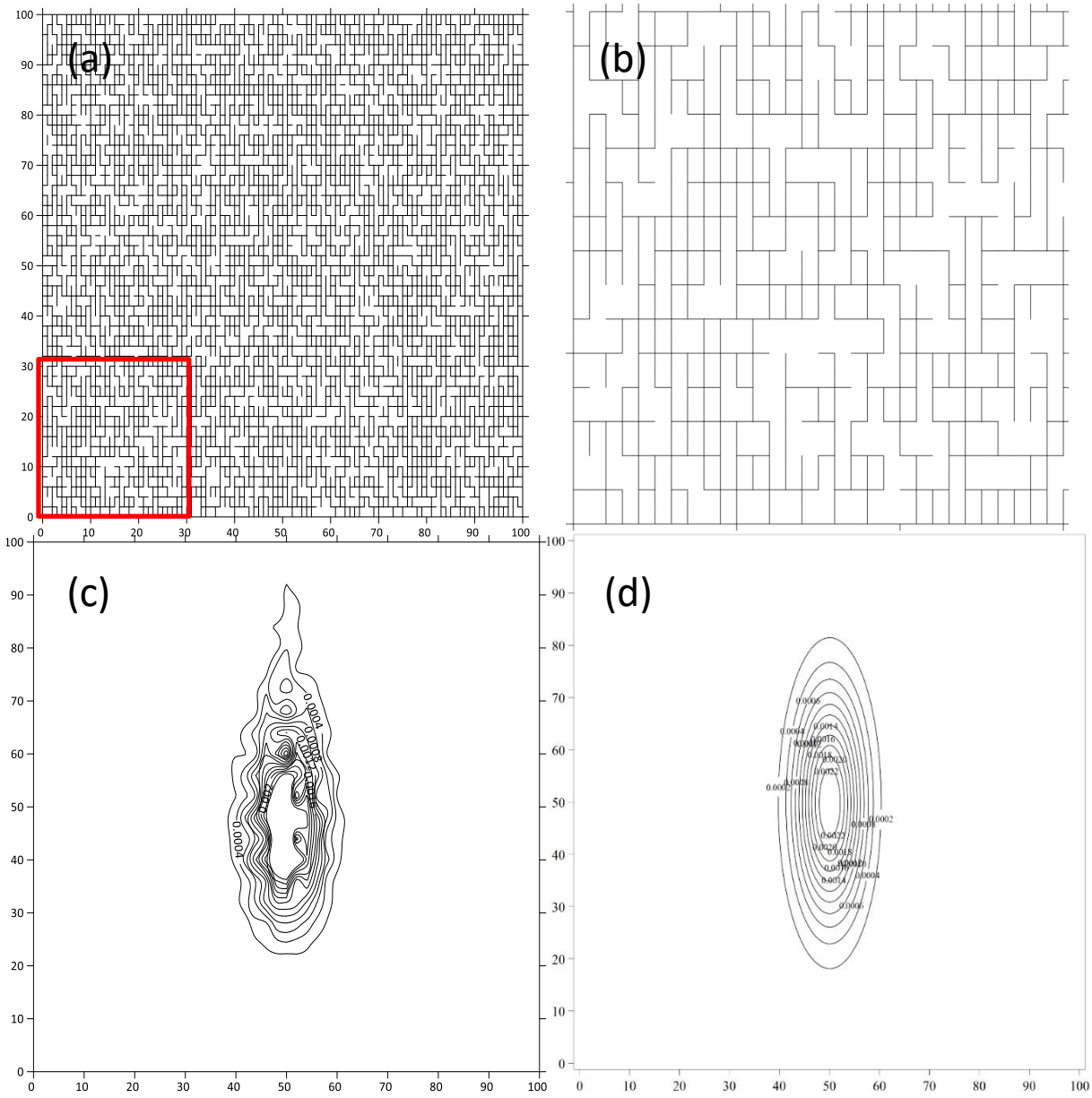

Figure. 6: Numerical simulation of particle transport through orthorhombic system where (a) is the lattice network, (b) is a zoomed in view of the selected area in (a), (c) is the bivariate Gaussian density of the synthetic plume, and (d) is the best-fit bivariate Gaussian density.

CHAPTER 5

DISCUSSION

Visual inspection of the three-dimensional densities provides additional insight on how these axial symmetries influence solute transport. The random selection of dispersivity values in the interval [0,10] further demonstrates differences between lower and higher symmetries denoted in the sensitivity analysis. Lower symmetry cases like orthorhombic, monoclinic, and triclinic contain a greater number of non-zero terms which lead to greater dispersion. For instance, comparing matrices 42 and 44, the only difference is the increase from two to six non-zero terms; however, D_{xx}, D_{yy}, D_{zz} increase from 3.5, 5.0, 3.5 to 13.38, 7.02, 4.60, respectively. This is an artifact of the random parameterization. In application, the amount of dispersion observed in the field will serve as a constraint when fitting each of the axial symmetry models to a contaminant plume. As noted in Chapter 3, this fitting exercise will need to account for both the dependence structure of the dispersivity terms (particularly for hexagonal and tetragonal) and the organization of these terms into groups. Given the greater number of non-zero terms, lower axial symmetries will likely utilize lower values of dispersivity than higher axial symmetries to yield the same values of dispersion.

Another difference between lower and higher axial symmetries is observed when the symmetry of the system reduces from isotropic to orthorhombic. This results in enhanced plume growth along a single primary transport direction while restricting plume growth along the other two directions. Fig. 4a - d illustrate how plume growth along the *x*-axis is enhanced as compared to growth along the *y*- and *z*-axes, during the progression from isotropic to orthorhombic symmetry. This pattern, however, does not exist in monoclinic and triclinic systems where plume growth can be significant along all axes (Fig. 4e and 4f). This is

explained by both the matrix structure and the organization of dispersivity terms into groups. In an orthorhombic system, all dispersivity terms in groups 2 and 3 are zero which concentrates dispersion along a single primary growth direction (Matrix 16). However, in monoclinic and triclinic cases non-zero terms are presented in the matrix for all four groups (Matrices 17 and 18).

The application of the framework to hexagonal-tetragonal and orthorhombic systems provides a pathway toward application of anisotropic tensors to geological systems. These two examples serve as a template for solving all non-zero tensorial dispersivity terms when constrained to plume variance. To our knowledge, this is the first instance in the literature where anisotropic dispersivity tensors are fully parameterized to a dataset. The strong correspondence between the numerical particle plumes (Fig. 5c, 6c) and best-fit bivariate Gaussian densities (Fig. 5d, 6d) further confirms the accuracy of the framework.

CHAPTER 6

CONCLUSION AND FUTURE WORK

6.1 Conclusion

A proposed framework for assessing the 4th rank dispersivity tensor under anisotropic axial symmetries is detailed in this study. This framework, which consists of analytic expressions, visualization of multi-dimensional Gaussian densities, and application of anisotropic tensor to numerical data, defines connections between dispersion, dispersivity, and velocity for non-isotropic dispersivity tensors. Analytic expressions are derived for triclinic (the most general case) in two-dimensions, and hexagonal, tetragonal, and orthorhombic in three-dimensions. Additional insight on the influence of individual dispersivity terms on dispersion for each of the axial symmetries were identified via sensitivity analyses and visualization of resultant multi-Gaussian densities. These findings include: (1) the influence of individual dispersivity terms on dispersion based on dependence of dispersivity terms, i.e., how the value of one term is connected to another term elsewhere in the tensor; (2) the structure of the matrix, which defines the number of non-zero values present in each of the four defined groups and how these groups contribute to Dxx, Dyy, and Dzz; and (3) plume growth becomes increasingly concentrated along the primary plume direction as symmetries progress from isotropic to orthorhombic, but is not present for the most general cases of monoclinic and triclinic. Numerical simulations of particle transport through hexagonal-tetragonal and orthorhombic symmetries systems are used to demonstrate the application of this framework to geological systems. A future study should utilize a broader range of parameter sets to generate synthetic data for evaluation and parameterization over the full range of axial symmetries presented in this work.

6.2 Future Work

The future work will utilize this framework to solve more real geological application problems.

6.2.1 Numerical Simulation on Hexagonal, Monoclinic and Triclinic Symmetries

Chapter 4.2 utilized lattice networks to generate plumes for application of the anisotropic dispersivity tensors to hexagonal-tetragonal and orthorhombic symmetries by incorporating. In the future, a broader range of parameter sets will be utilized to generate synthetic data for evaluation and parameterization over the full range of axial symmetries presented in this work.

6.2.2 Borden Landfill

Another potential future work is the Borden Landfill plume. Borden Landfill is one of the best-known subsurface contaminant transport test fields, which is located on the Canadian Forces Base in Borden, Ontario (Fetter, 1999). Mackay et al. (1986) conducted a natural gradient slug injection field experiment, and observed the concentration distribution of the chloride ion and carbon tetrachloride after a period of time. After that, a lot of studies have been performed to simulate the plume transports. The framework developed in this manuscript can be applied to this Borden Landfill plume study. The solute concentration at a certain point is described by Eq. 41:

$$C(x,y,z;x',y',z') = \frac{C_0}{2\sigma_x\sigma_y\sigma_z\sqrt{2\pi}} \cdot exp\left(-\frac{(x-x')^2}{2\sigma_x^2} - \frac{(y-y')^2}{2\sigma_y^2} - \frac{(z-z')^2}{2\sigma_z^2}\right).$$

After identifying the most suitable symmetry case, dispersion (σ) in this equation can be solved by using the method in Chapter 2.3. The shape of the plume can be predicted by the method used in Chapter as well. This provides a different approach to simulate the plume transports in the field.

Appendix A

DISPERSION VALUES

For two-dimensional Triclinic case,

$$\lambda_1=\frac{1}{2}(a_{11}V_1+a_{12}V_1+a_{13}V_2+a_{14}V_2+a_{21}V_1+a_{22}V_1+a_{23}V_2+a_{24}V_2)+\frac{1}{2}(a_{11}^2V_1^2+$$

$$2a_{11}a_{12}V_1^2+2a_{11}a_{13}V_1V_2+2a_{11}a_{14}V_1V_2-2a_{11}a_{21}V_1^2-2a_{11}a_{22}V_1^2-2a_{11}a_{23}V_1V_2-$$

$$2a_{11}a_{24}V_1V_2+2a_{12}^2V_1^2+2a_{12}a_{13}V_1V_2+2a_{12}a_{14}V_1V_2-2a_{12}a_{21}V_1^2-2a_{12}a_{22}V_1^2-$$

$$2a_{12}a_{23}V_1V_2-2a_{12}a_{24}V_1V_2+a_{13}^2V_2^2+2a_{13}a_{14}V_2^2-2a_{13}a_{21}V_1V_2-2a_{13}a_{22}V_1V_2-$$

$$2a_{13}a_{23}V_1^2-2a_{13}a_{24}V_2^2+a_{14}^2V_2^2-2a_{14}a_{21}V_1V_2-2a_{14}a_{22}V_1V_2-2a_{14}a_{23}V_2^2-$$

$$2a_{14}a_{24}V_2^2+a_{21}^2V_1^2+2a_{21}a_{22}V_1^2+2a_{21}a_{23}V_1V_2+2a_{11}a_{24}V_1V_2+a_{22}^2V_1^2+$$

$$2a_{22}a_{23}V_1V_2+2a_{22}a_{24}V_1V_2+a_{23}^2V_2^2+2a_{23}a_{24}V_2^2+a_{24}^2V_2^2+4a_{31}a_{41}V_1^2+4a_{31}a_{42}V_1^2+$$

$$4a_{31}a_{43}V_1V_2+4a_{31}a_{44}V_1V_2+4a_{32}a_{41}V_1^2+4a_{32}a_{42}V_1^2+4a_{32}a_{43}V_1V_2+4a_{32}a_{44}V_1V_2+$$

$$4a_{33}a_{41}V_1V_2+4a_{33}a_{42}V_1V_2+4a_{33}a_{43}V_2^2+4a_{33}a_{44}V_2^2+4a_{34}a_{41}V_1V_2+4a_{34}a_{42}V_1V_2+$$

$$4a_{34}a_{43}V_2^2+4a_{34}a_{44}V_2^2)^{\frac{1}{2}}$$

$$\lambda_2=\frac{1}{2}(a_{11}V_1+a_{12}V_1+a_{13}V_2+a_{14}V_2+a_{21}V_1+a_{22}V_1+a_{23}V_2+a_{24}V_2)-$$

$$\frac{1}{2}(a_{11}^2V_1^2+2a_{11}a_{12}V_1^2+2a_{11}a_{13}V_1V_2+2a_{11}a_{14}V_1V_2-2a_{11}a_{21}V_1^2-2a_{11}a_{22}V_1^2-$$

$$2a_{11}a_{23}V_1V_2-2a_{11}a_{24}V_1V_2+2a_{12}^2V_1^2+2a_{12}a_{13}V_1V_2+2a_{12}a_{14}V_1V_2-2a_{12}a_{21}V_1^2-$$

$$2a_{12}a_{22}V_1^2-2a_{12}a_{23}V_1V_2-2a_{12}a_{24}V_1V_2+a_{13}^2V_2^2+2a_{13}a_{14}V_2^2-2a_{13}a_{21}V_1V_2-$$

$$2a_{13}a_{22}V_1V_2-2a_{13}a_{23}V_1^2-2a_{13}a_{24}V_2^2+a_{14}^2V_2^2-2a_{14}a_{21}V_1V_2-2a_{14}a_{22}V_1V_2-$$

$$2a_{14}a_{23}V_2^2-2a_{14}a_{24}V_2^2+a_{21}^2V_1^2+2a_{21}a_{22}V_1^2+2a_{21}a_{23}V_1V_2+2a_{11}a_{24}V_1V_2+a_{22}^2V_1^2+$$

$$2a_{22}a_{23}V_1V_2+2a_{22}a_{24}V_1V_2+a_{23}^2V_2^2+2a_{23}a_{24}V_2^2+a_{24}^2V_2^2+4a_{31}a_{41}V_1^2+4a_{31}a_{42}V_1^2+$$

$$4a_{31}a_{43}V_1V_2+4a_{31}a_{44}V_1V_2+4a_{32}a_{41}V_1^2+4a_{32}a_{42}V_1^2+4a_{32}a_{43}V_1V_2+4a_{32}a_{44}V_1V_2+$$

$$4a_{33}a_{41}V_1V_2+4a_{33}a_{42}V_1V_2+4a_{33}a_{43}V_2^2+4a_{33}a_{44}V_2^2+4a_{34}a_{41}V_1V_2+4a_{34}a_{42}V_1V_2+$$

$$4a_{34}a_{43}V_2^2+4a_{34}a_{44}V_2^2)^{\frac{1}{2}}$$

For three-dimensional Hexagonal case,

$$\lambda_1 = \frac{1}{3\sqrt[3]{2}}\left(\left(-2a^3+6a^2b+\left(4\left(-a^2+2ab-b^2-3c^2-3d^2-3e^2\right)^3+\left(-2a^3+6a^2b-6ab^2+18ac^2-9ad^2-9ae^2+2b^3-18bc^2+9bd^2+9be^2+54cde\right)^2\right)^{\frac{1}{2}}-6ab^2+18ac^2-9ad^2-9ae^2+2b^3-18bc^2+9bd^2+9be^2+54cde\right)^{\frac{1}{3}}\right)-\left(\sqrt[3]{2}\left(-a^2+2ab-b^2-3c^2-3d^2-3e^2\right)\right)/\left(3\left(-2a^3+6a^2b+\left(4\left(-a^2+2ab-b^2-3c^2-3d^2-3e^2\right)^3+\left(-2a^3+6a^2b-6ab^2+18ac^2-9ad^2-9ae^2+2b^3-18bc^2+9bd^2+9be^2+54cde\right)^2\right)^{\frac{1}{2}}-6ab^2+18ac^2-9ad^2-9ae^2+2b^3-18bc^2+9bd^2+9be^2+54cde\right)^{\frac{1}{3}}\right)+\frac{2a+b}{3}$$

$$\lambda_2 = -\frac{1}{6\sqrt[3]{2}}\left(1-i\sqrt{3}\right)\left(\left(-2a^3+6a^2b+\left(4\left(-a^2+2ab-b^2-3c^2-3d^2-3e^2\right)^3+\left(-2a^3+6a^2b-6ab^2+18ac^2-9ad^2-9ae^2+2b^3-18bc^2+9bd^2+9be^2+54cde\right)^2\right)^{\frac{1}{2}}-6ab^2+18ac^2-9ad^2-9ae^2+2b^3-18bc^2+9bd^2+9be^2+54cde\right)^{\frac{1}{3}}\right)+\left(\left(1+i\sqrt{3}\right)\left(-a^2+2ab-b^2-3c^2-3d^2-3e^2\right)\right)/\left(3\sqrt[3]{4}\left(-2a^3+6a^2b+\left(4\left(-a^2+2ab-b^2-3c^2-3d^2-3e^2\right)^3+\left(-2a^3+6a^2b-6ab^2+18ac^2-9ad^2-9ae^2+2b^3-18bc^2+9bd^2+9be^2+54cde\right)^2\right)^{\frac{1}{2}}-6ab^2+18ac^2-9ad^2-9ae^2+2b^3-18bc^2+9bd^2+9be^2+54cde\right)^{\frac{1}{3}}\right)+\frac{2a+b}{3}$$

$$\lambda_3 = -\frac{1}{6\sqrt[3]{2}}\left(1+i\sqrt{3}\right)\left(\left(-2a^3+6a^2b+\left(4\left(-a^2+2ab-b^2-3c^2-3d^2-3e^2\right)^3+\left(-2a^3+6a^2b-6ab^2+18ac^2-9ad^2-9ae^2+2b^3-18bc^2+9bd^2+9be^2+54cde\right)^2\right)^{\frac{1}{2}}-6ab^2+18ac^2-9ad^2-9ae^2+2b^3-18bc^2+9bd^2+9be^2+54cde\right)^{\frac{1}{3}}\right)+\left(\left(1-i\sqrt{3}\right)\left(-a^2+2ab-b^2-3c^2-3d^2-3e^2\right)\right)/\left(3\sqrt[3]{4}\left(-2a^3+6a^2b+\left(4\left(-a^2+2ab-b^2-3c^2-3d^2-3e^2\right)^3+\left(-2a^3+6a^2b-6ab^2+18ac^2-9ad^2-\right.\right.\right.$$

$9ae^2 + 2b^3 - 18bc^2 + 9bd^2 + 9be^2 + 54cde)^2)^{\frac{1}{2}} - 6ab^2 + 18ac^2 - 9ad^2 - 9ae^2 +$

$2b^3 - 18bc^2 + 9bd^2 + 9be^2 + 54cde)^{\frac{1}{3}}) + \frac{2a+b}{3}$

For three-dimensional Tetragonal case,

$\lambda_1 = \frac{1}{3\sqrt[3]{2}}(\Big(-2a^3 + 6a^2b + (4(-a^2 + 2ab - b^2 - 3c^2 - 3d^2 - 3e^2)^3 + (-2a^3 + 6a^2b -$

$6ab^2 + 18ac^2 - 9ad^2 - 9ae^2 + 2b^3 - 18bc^2 + 9bd^2 + 9be^2 + 54cde)^2)^{\frac{1}{2}} -$

$6ab^2 + 18ac^2 - 9ad^2 - 9ae^2 + 2b^3 - 18bc^2 + 9bd^2 + 9be^2 + 54cde)^{\frac{1}{3}}\Big) -$

$(\sqrt[3]{2}(-a^2 + 2ab - b^2 - 3c^2 - 3d^2 - 3e^2))/(3(-2a^3 + 6a^2b + (4(-a^2 + 2ab - b^2 -$

$3c^2 - 3d^2 - 3e^2)^3 + (-2a^3 + 6a^2b - 6ab^2 + 18ac^2 - 9ad^2 - 9ae^2 + 2b^3 - 18bc^2 +$

$9bd^2 + 9be^2 + 54cde)^2)^{\frac{1}{2}} - 6ab^2 + 18ac^2 - 9ad^2 - 9ae^2 + 2b^3 - 18bc^2 + 9bd^2 +$

$9be^2 + 54cde)^{\frac{1}{3}}) + \frac{2a+b}{3}$

$\lambda_2 = -\frac{1}{6\sqrt[3]{2}}(1 - i\sqrt{3})(\Big(-2a^3 + 6a^2b + (4(-a^2 + 2ab - b^2 - 3c^2 - 3d^2 - 3e^2)^3 +$

$(-2a^3 + 6a^2b - 6ab^2 + 18ac^2 - 9ad^2 - 9ae^2 + 2b^3 - 18bc^2 + 9bd^2 + 9be^2 +$

$54cde)^2)^{\frac{1}{2}} - 6ab^2 + 18ac^2 - 9ad^2 - 9ae^2 + 2b^3 - 18bc^2 + 9bd^2 + 9be^2 +$

$54cde)^{\frac{1}{3}}\Big) + ((1 + i\sqrt{3})(-a^2 + 2ab - b^2 - 3c^2 - 3d^2 - 3e^2))/(3\sqrt[3]{4}(-2a^3 + 6a^2b +$

$(4(-a^2 + 2ab - b^2 - 3c^2 - 3d^2 - 3e^2)^3 + (-2a^3 + 6a^2b - 6ab^2 + 18ac^2 - 9ad^2 -$

$9ae^2 + 2b^3 - 18bc^2 + 9bd^2 + 9be^2 + 54cde)^2)^{\frac{1}{2}} - 6ab^2 + 18ac^2 - 9ad^2 - 9ae^2 +$

$2b^3 - 18bc^2 + 9bd^2 + 9be^2 + 54cde)^{\frac{1}{3}}) + \frac{2a+b}{3}$

$\lambda_3 = -\frac{1}{6\sqrt[3]{2}}(1 + i\sqrt{3})(\Big(-2a^3 + 6a^2b + (4(-a^2 + 2ab - b^2 - 3c^2 - 3d^2 - 3e^2)^3 +$

$(-2a^3 + 6a^2b - 6ab^2 + 18ac^2 - 9ad^2 - 9ae^2 + 2b^3 - 18bc^2 + 9bd^2 + 9be^2 +$

$54cde)^2)^{\frac{1}{2}} - 6ab^2 + 18ac^2 - 9ad^2 - 9ae^2 + 2b^3 - 18bc^2 + 9bd^2 + 9be^2 +$

$54cde)^{\frac{1}{3}}\Big) + ((1 - i\sqrt{3})(-a^2 + 2ab - b^2 - 3c^2 - 3d^2 - 3e^2))/(3\sqrt[3]{4}(-2a^3 + 6a^2b +$

$(4(-a^2 + 2ab - b^2 - 3c^2 - 3d^2 - 3e^2)^3 + (-2a^3 + 6a^2b - 6ab^2 + 18ac^2 - 9ad^2 -$

$9ae^2 + 2b^3 - 18bc^2 + 9bd^2 + 9be^2 + 54cde)^2)^{\frac{1}{2}} - 6ab^2 + 18ac^2 - 9ad^2 - 9ae^2 +$

$2b^3 - 18bc^2 + 9bd^2 + 9be^2 + 54cde)^{\frac{1}{3}}) + \frac{2a+b}{3}$.

For three-dimensional Orthorhombic case,

$\lambda_1 = \frac{1}{3\sqrt[3]{2}}(\Big(2a^3 - 3a^2b - 3a^2c + (4(-a^2 + ab + ac - b^2 + bc - c^2 - 3d^2 - 3e^2 -$

$3f^2)^3 + (2a^3 - 3a^2b - 3a^2c - 3ab^2 + 12abc - 3ac^2 + 9ad^2 - 18ae^2 + 9af^2 + 2b^3 -$

$3b^2c - 3bc^2 + 9bd^2 + 9be^2 - 18bf^2 + 2c^2 - 18cd^2 + 9ce^2 + 9cf^2 + 54def)^2)^{\frac{1}{2}} -$

$6ab^2 + 9ac^2 - 9ad^2 + 2b^3 - 9bc^2 + 9bd^2 + 54def)^{\frac{1}{3}}\Big) - (\sqrt[3]{2}(-a^2 + 2ab + ac - b^2 +$

$bc - c^2 - 3d^2 - 3e^2 - 3f^2))/(3(2a^3 - 3a^2b - 3a^2c + (4(-a^2 + ab + ac - b^2 + bc -$

$c^2 - 3d^2 - 3e^2 - 3f^2)^3 + (2a^3 - 3a^2b - 3a^2c - 3ab^2 + 12abc - 3ac^2 + 9ad^2 -$

$18ae^2 + 9af^2 + 2b^3 - 3b^2c - 3bc^2 + 9bd^2 + 9be^2 - 18bf^2 + 2c^2 - 18cd^2 + 9ce^2 +$

$9cf^2 + 54def)^2)^{\frac{1}{2}} - 6ab^2 + 9ac^2 - 9ad^2 + 2b^3 - 9bc^2 + 9bd^2 + 54def)^{\frac{1}{3}}) + \frac{a+b+c}{3}$

$\lambda_2 = -\frac{1}{6\sqrt[3]{2}}(1 - i\sqrt{3})(\Big(2\mathrm{a}^3 - 3\mathrm{a}^2\mathrm{b} - 3\mathrm{a}^2\mathrm{c} + (4(-a^2 + ab + ac - b^2 + bc - c^2 - 3d^2 -$

$3e^2 - 3f^2)^3 + (2\mathrm{a}^3 - 3\mathrm{a}^2\mathrm{b} - 3\mathrm{a}^2\mathrm{c} - 3\mathrm{ab}^2 + 12\mathrm{abc} - 3\mathrm{ac}^2 + 9\mathrm{ad}^2 - 18\mathrm{ae}^2 + 9\mathrm{af}^2 +$

$2\mathrm{b}^3 - 3\mathrm{b}^2\mathrm{c} - 3\mathrm{bc}^2 + 9\mathrm{bd}^2 + 9\mathrm{be}^2 - 18\mathrm{bf}^2 + 2\mathrm{c}^2 - 18\mathrm{cd}^2 + 9\mathrm{ce}^2 + 9\mathrm{cf}^2 + 54\mathrm{def})^2)^{\frac{1}{2}} -$

$6\mathrm{ab}^2 + 9\mathrm{ac}^2 - 9\mathrm{ad}^2 + 2\mathrm{b}^3 - 9\mathrm{bc}^2 + 9\mathrm{bd}^2 + 54\mathrm{def})^{\frac{1}{3}}\Big) + ((1 + i\sqrt{3})(-\mathrm{a}^2 + 2\mathrm{ab} + \mathrm{ac} -$

$\mathrm{b}^2 + \mathrm{bc} - \mathrm{c}^2 - 3\mathrm{d}^2 - 3\mathrm{e}^2 - 3\mathrm{f}^2))/(3\sqrt[3]{4}(2\mathrm{a}^3 - 3\mathrm{a}^2\mathrm{b} - 3\mathrm{a}^2\mathrm{c} + (4(-a^2 + ab + ac - b^2 +$

$bc - c^2 - 3d^2 - 3e^2 - 3f^2)^3 + (2\mathrm{a}^3 - 3\mathrm{a}^2\mathrm{b} - 3\mathrm{a}^2\mathrm{c} - 3\mathrm{ab}^2 + 12\mathrm{abc} - 3\mathrm{ac}^2 + 9\mathrm{ad}^2 -$

$18\mathrm{ae}^2 + 9\mathrm{af}^2 + 2\mathrm{b}^3 - 3\mathrm{b}^2\mathrm{c} - 3\mathrm{bc}^2 + 9\mathrm{bd}^2 + 9\mathrm{be}^2 - 18\mathrm{bf}^2 + 2\mathrm{c}^2 - 18\mathrm{cd}^2 + 9\mathrm{ce}^2 +$

$9\mathrm{cf}^2 + 54\mathrm{def})^2)^{\frac{1}{2}} - 6\mathrm{ab}^2 + 9\mathrm{ac}^2 - 9\mathrm{ad}^2 + 2\mathrm{b}^3 - 9\mathrm{bc}^2 + 9\mathrm{bd}^2 + 54\mathrm{def})^{\frac{1}{3}}) + \frac{\mathrm{a+b+c}}{3}$

$$\lambda_3 = -\frac{1}{6\sqrt[3]{2}}(1+i\sqrt{3})\Big(\Big(2a^3-3a^2b-3a^2c+(4(-a^2+ab+ac-b^2+bc-c^2-3d^2-3e^2-3f^2)^3+(2a^3-3a^2b-3a^2c-3ab^2+12abc-3ac^2+9ad^2-18ae^2+9af^2+2b^3-3b^2c-3bc^2+9bd^2+9be^2-18bf^2+2c^2-18cd^2+9ce^2+9cf^2+54def)^2)^{\frac{1}{2}}-6ab^2+9ac^2-9ad^2+2b^3-9bc^2+9bd^2+54def)^{\frac{1}{3}}\Big)+((1-i\sqrt{3})(-a^2+2ab+ac-b^2+bc-c^2-3d^2-3e^2-3f^2))/(3\sqrt[3]{4}(2a^3-3a^2b-3a^2c+(4(-a^2+ab+ac-b^2+bc-c^2-3d^2-3e^2-3f^2)^3+(2a^3-3a^2b-3a^2c-3ab^2+12abc-3ac^2+9ad^2-18ae^2+9af^2+2b^3-3b^2c-3bc^2+9bd^2+9be^2-18bf^2+2c^2-18cd^2+9ce^2+9cf^2+54def)^2)^{\frac{1}{2}}-6ab^2+9ac^2-9ad^2+2b^3-9bc^2+9bd^2+54def)^{\frac{1}{3}})+\frac{a+b+c}{3}$$

Appendix B

VALIDATION PROCESS

Based on calculation:

$$D_{11} = \left(\frac{a_{11}v_1}{2} + \frac{a_{12}v_1}{2} + \frac{a_{13}v_2}{2} + \frac{a_{14}v_2}{2} + \frac{a_{21}v_1}{2} + \frac{a_{22}v_1}{2} + \frac{a_{23}v_2}{2} + \frac{a_{24}v_2}{2}\right) + \frac{1}{2}(a_{11}^2v_1^2 + 2a_{11}a_{12}v_1^2 + 2a_{11}a_{13}v_1v_2 + 2a_{11}a_{14}v_1v_2 - 2a_{11}a_{21}v_1^2 - 2a_{11}a_{22}v_1^2 - 2a_{11}a_{23}v_1v_2 - 2a_{11}a_{24}v_1v_2 + a_{12}^2v_1^2 + 2a_{12}a_{13}v_1v_2 + 2a_{12}a_{14}v_1v_2 - 2a_{12}a_{21}v_1^2 - 2a_{12}a_{22}v_1^2 - 2a_{12}a_{23}v_1v_2 - 2a_{12}a_{24}v_1v_2a_{13}^2v_2^2 + 2a_{13}a_{14}v_2^2 - 2a_{13}a_{21}v_1v_2 - 2a_{13}a_{22}v_1v_2 - 2a_{13}a_{23}v_2^2 - 2a_{13}a_{24}v_2^2 + a_{14}^2v_2^2 - 2a_{14}a_{21}v_1v_2 - 2a_{14}a_{22}v_1v_2 - 2a_{14}a_{23}v_2^2 - 2a_{14}a_{24}v_2^2 + a_{21}^2v_1^2 + 2a_{21}a_{22}v_1^2 + 2a_{21}a_{23}v_1v_2 + 2a_{21}a_{24}v_1v_2 + a_{22}^2v_1^2 + 2a_{22}a_{23}v_1v_2 + 2a_{22}a_{24}v_1v_2 + a_{23}^2v_2^2 + 2a_{23}a_{24}v_2^2 + a_{24}^2v_2^2 + 4a_{31}a_{41}v_1^2 + 4a_{31}a_{42}v_1^2 + 4a_{31}a_{43}v_1v_2 + 4a_{31}a_{44}v_1v_2 + 4a_{32}a_{41}v_1^2 + 4a_{32}a_{42}v_1^2 + 4a_{32}a_{43}v_1v_2 + 4a_{32}a_{44}v_1v_2 + 4a_{33}a_{41}v_1v_2 + 4a_{33}a_{42}v_1v_2 + 4a_{33}a_{43}v_2^2 + 4a_{33}a_{44}v_2^2 + 4a_{34}a_{41}v_1v_2 + 4a_{34}a_{42}v_1v_2 + 4a_{34}a_{43}v_2^2 + 4a_{34}a_{44}v_2^2)^{\frac{1}{2}}$$

$$D_{22} = \left(\frac{a_{11}v_1}{2} + \frac{a_{12}v_1}{2} + \frac{a_{13}v_2}{2} + \frac{a_{14}v_2}{2} + \frac{a_{21}v_1}{2} + \frac{a_{22}v_1}{2} + \frac{a_{23}v_2}{2} + \frac{a_{24}v_2}{2}\right) - \frac{1}{2}(a_{11}^2v_1^2 + 2a_{11}a_{12}v_1^2 + 2a_{11}a_{13}v_1v_2 + 2a_{11}a_{14}v_1v_2 - 2a_{11}a_{21}v_1^2 - 2a_{11}a_{22}v_1^2 - 2a_{11}a_{23}v_1v_2 - 2a_{11}a_{24}v_1v_2 + a_{12}^2v_1^2 + 2a_{12}a_{13}v_1v_2 + 2a_{12}a_{14}v_1v_2 - 2a_{12}a_{21}v_1^2 - 2a_{12}a_{22}v_1^2 - 2a_{12}a_{23}v_1v_2 - 2a_{12}a_{24}v_1v_2a_{13}^2v_2^2 + 2a_{13}a_{14}v_2^2 - 2a_{13}a_{21}v_1v_2 - 2a_{13}a_{22}v_1v_2 - 2a_{13}a_{23}v_2^2 - 2a_{13}a_{24}v_2^2 + a_{14}^2v_2^2 - 2a_{14}a_{21}v_1v_2 - 2a_{14}a_{22}v_1v_2 - 2a_{14}a_{23}v_2^2 - 2a_{14}a_{24}v_2^2 + a_{21}^2v_1^2 + 2a_{21}a_{22}v_1^2 + 2a_{21}a_{23}v_1v_2 + 2a_{21}a_{24}v_1v_2 + a_{22}^2v_1^2 + 2a_{22}a_{23}v_1v_2 + 2a_{22}a_{24}v_1v_2 + a_{23}^2v_2^2 + 2a_{23}a_{24}v_2^2 + a_{24}^2v_2^2 + 4a_{31}a_{41}v_1^2 + 4a_{31}a_{42}v_1^2 + 4a_{31}a_{43}v_1v_2 + 4a_{31}a_{44}v_1v_2 + 4a_{32}a_{41}v_1^2 + 4a_{32}a_{42}v_1^2 + 4a_{32}a_{43}v_1v_2 + 4a_{32}a_{44}v_1v_2 + 4a_{33}a_{41}v_1v_2 + 4a_{33}a_{42}v_1v_2 + 4a_{33}a_{43}v_2^2 + 4a_{33}a_{44}v_2^2 + 4a_{34}a_{41}v_1v_2 + 4a_{34}a_{42}v_1v_2 + 4a_{34}a_{43}v_2^2 + 4a_{34}a_{44}v_2^2)^{\frac{1}{2}}$$

$$D_{ij} = \begin{vmatrix} \lambda_1 & 0 \\ 0 & \lambda_2 \end{vmatrix}.$$

Following the validation process, first step is calculating $D_{ij} = a_{ijkl} \frac{V_k V_l}{v}$ directly. Mark the result as D_{ij1}.

Defining a two-dimensional triclinic dispersivity tensor in accordance with matrix 26:

$$a_{ijkl} = \begin{vmatrix} 13 & 14 & 15 & 16 \\ 9 & 10 & 11 & 12 \\ 5 & 6 & 7 & 8 \\ 1 & 2 & 3 & 4 \end{vmatrix}. \quad (63)$$

And velocity tensor:

$$V_k V_l = \begin{vmatrix} 1 \\ 1 \\ 1 \\ 1 \end{vmatrix}. \quad (64)$$

$$\Rightarrow D_{ij1} = \begin{vmatrix} 58 & 26 \\ 10 & 42 \end{vmatrix}. \quad (65)$$

Rewriting to:

$$D_{ij1} = \begin{vmatrix} 68 & 0 \\ 0 & 32 \end{vmatrix}. \quad (66)$$

Second step is calculating D_{ij} from the derived analytical expressions. Mark the result as D_{ij2}.

$a_{11} = 16$, $a_{12} = 15$, $a_{13} = 14$, $a_{14} = 13$, $a_{21} = 12$, $a_{22} = 11$, $a_{23} = 10$, $a_{24} = 9$, $a_{31} = 8$, $a_{32} = 7$, $a_{33} = 6$, $a_{34} = 5$, $a_{41} = 4$, $a_{42} = 3$, $a_{43} = 2$, $a_{44} = 1$, $v_k = 1$, $v_l = 1$ (matrices 54 and 55).

Putting a_{ijkl}, v_k, v_l value back to D_{11} and D_{22}:

$$\begin{aligned} D_{11} &= \left\lceil 50 + \frac{\sqrt{1296}}{2} \right\rceil = 68 \\ D_{22} &= \left\lceil 50 - \frac{\sqrt{1296}}{2} \right\rceil = 32 \end{aligned} \quad (67)$$

$$\Rightarrow D_{ij2} = \begin{vmatrix} 68 & 0 \\ 0 & 32 \end{vmatrix}. \tag{68}$$

Lastly, subtract D_{ij1} from D_{ij2}:

$$D_{ij1} - D_{ij2} = \begin{vmatrix} 68-68 & 0-0 \\ 0-0 & 32-32 \end{vmatrix} = \begin{vmatrix} 0 & 0 \\ 0 & 0 \end{vmatrix}. \tag{69}$$

Since it equals 0, the calculation is correct.

Running another round of test.

Defining a two-dimensional triclinic dispersivity tensor in accordance with matrix 26:

$$a_{ijkl} = \begin{vmatrix} 23 & 5 & 25 & 26 \\ 19 & 20 & 31 & 22 \\ 12 & 15 & 17 & 9 \\ 3 & 1 & 7 & 6 \end{vmatrix}. \tag{70}$$

Velocity tensor:

$$V_k V_l = \begin{vmatrix} 2 \\ 2 \\ 3 \\ 3 \end{vmatrix}. \tag{71}$$

$$\Rightarrow D_{ij1} = \begin{vmatrix} 303 & 0 \\ 0 & 143 \end{vmatrix}. \tag{72}$$

Calculating D_{ij2}: $a_{11} = 23$, $a_{12} = 5$, $a_{13} = 25$, $a_{14} = 26$, $a_{21} = 19$, $a_{22} = 20$, $a_{23} = 31$, $a_{24} = 22$, $a_{31} = 12$, $a_{32} = 15$ $a_{33} = 17$, $a_{34} = 9$, $a_{41} = 3$, $a_{42} = 1$, $a_{43} = 7$, $a_{44} = 6$, $v_k = 2$, $v_l = 3$ (matrices 61 and 62). Result is:

$$\begin{aligned} D_{11} &= 223 + \frac{\sqrt{25600}}{2} = 303 \\ D_{22} &= 223 - \frac{\sqrt{25600}}{2} = 143 \end{aligned} \tag{73}$$

$$\Rightarrow D_{ij2} = \begin{vmatrix} 303 & 0 \\ 0 & 143 \end{vmatrix}. \tag{74}$$

Subtracting D_{ij1} from D_{ij2}:

$$D_{ij1} - D_{ij2} = \begin{vmatrix} 0 & 0 \\ 0 & 0 \end{vmatrix}. \tag{75}$$

Result equals 0.

REFERENCES

Bear J (1961) On the tensor form of dispersion in porous media. Journal of Geophysical Research 66(4):1185--1197

Bear J (1972) Dynamics of Fluids in Porous Media. Courier Corporation

Bear J, Fel L, Zimmels Y (2009) Effects of material symmetry on the coefficients of transport in anisotropic porous media. Transport in Porous Media 82. https://doi.org/10.1007/s11242-009-9430-1

Bruhn RL, Parry WT, Yonkee WA, et al (1994) Fracturing and hydrothermal alteration in normal fault zones. Pure and Applied Geophysics 142:609--644. https://doi.org/10.1007/BF00876057

Caine JS, Evans JP, Forster CB (1996) {Fault zone architecture and permeability structure}. Geology 24(11):1025--1028. https://doi.org/10.1130/0091-7613(1996)024<1025:FZAAPS>2.3.CO;2

Day PR (1956) Dispersion of a moving salt-water boundary advancing through saturated sand. Eos, Transactions American Geophysical Union 37(5):595--601

Fel LG, Bear J (2009) Dispersion and dispersivity tensors in saturated porous media with uniaxial symmetry. Transport in Porous Media 85:259--268. https://doi.org/10.1007/s11242-010-9558-z

Ferrill, D. A. (1999). Stressed rock strains groundwater at Yucca Mountain, Nevada. GSA Today, 9(5), 1-8.

Fetter, C. W. (1999). Contaminant hydrogeology. United Kingdom: Prentice Hall.

Johri M, Zoback MD, Hennings P (2014) A scaling law to characterize fault-damage zones at reservoir depths. AAPG Bulletin 98(10):2057--2079. https://10.1306/05061413173

Klimczak C, Schultz RA, Parashar R & Donald M. Reeves (2010) Cubic law with aperture-length correlation: implications for network scale fluid flow. Hydrogeology Journal 18:851--862. https://doi.org/10.1007/s10040-009-0572-6

Lee SY, Carle SF, Fogg GE (2007) Geologic heterogeneity and a comparison of two geostatistical models: Sequential gaussian and transition probability-based geostatistical simulation. Advances in Water Resources 30(9):1914--1932. https://doi.org/10.1016/j.advwatres.2007.03.005

Mackay, D. M., Freyberg, D. L., Roberts, P. V., & Cherry, J. A. (1986). A natural gradient experiment on solute transport in a sand aquifer: 1. Approach and overview of plume movement. Water Resources Research, 22(13), 2017-2029.

Oda M, Hatsuyama Y, Ohnishi Y (1987) Numerical experiments on permeability tensor and its application to jointed granite at Stripa mine, Sweden. Journal of Geophysical Research: Solid Earth 92(B8):8037--8048. https://doi.org/10.1029/JB092iB08p08037

Parashar, R., & Reeves, D.M. (2012). On iterative techniques for computing flow in large two-dimensional discrete fracture networks. J. Comput. Appl. Math., 236, 4712-4724.

Pickup G, Ringrose P, Jensen J, et al (1994) Permeability tensors for sedimentary structures. Mathematical Geology 26:227--250. https://10.1007/BF02082765

Reeves, D.M., R. Parashar, and Y. Zhang (2012), Hydrogeologic characterization of fractured rock masses intended for disposal of radioactive waste, In: Radioactive Waste, Ed. R.A. Rahman, InTech Publishing, ISBN 978-953-51-0551-0.

Rifai, Eddine MN, Kaufman WJ, et al. (1956) Dispersion phenomena in laminar flow through porous media. Berkeley, Calif: University of California

Sahini, M., & Sahimi, M. (1994). Applications of percolation theory. Taylor & Francis

Scheidegger AE (1954) Statistical hydrodynamics in porous media. Journal of Applied Physics 25(8):994--1001

Scheidegger AE (1957) On the theory of flow of miscible phases in porous media. IAH Assembly of Toronto 2:236--242

Scheidegger AE (1958) The physics of flow through porous media. Soil Science 86(6):355

Scheidegger AE (1961) General theory of dispersion in porous media. Journal of Geophysical Research 66:3273--3278

Sirotin I, Shaskolskaia M (1982) Fundamentals of Crystal Physics. Mir Publishers